COMPOUND LASER MODES OF MUTUALLY DELAY-COUPLED LASERS

HARTMUT ERZGRÄBER*, BERND KRAUSKOPF†, AND DAAN LENSTRA‡

November 2004

Abstract. We consider a model of two mutually delay-coupled semiconductor lasers in a face to face configuration. The lasers are coherently coupled via their optical fields, where the time delay τ arises from the finite propagation time of the light from one laser to the other. This system is described well by single mode rate equations, which are a system of delay differential equations (DDEs) with one fixed delay.

We study the compound laser modes (CLMs) of the system, where both lasers operate at an identical, time-independant frequency. By making use of numerical continuation applied to the full DDEs, we present a comprehensive geometrical picture of how CLMs depend on the two main physical parameters, namely the coupling phase and the detuning between the two lasers. The different branches of CLMs are organized by unfoldings of pitchfork bifurcations that exist for zero detuning. As a function of the detuning, different branches of CLMs connect, split or disappear in transitions through codimension-one singularities in the surface of CLMs.

Key words. mutually delay-coupled lasers, delay differential equations, numerical continuation, symmetry breaking, singularity

AMS subject classifications. 15A15, 15A09, 15A23

1. Introduction. In this paper we consider a simple setup of two mutually delay-coupled semiconductor lasers in a face-to-face configuration. The system is sketched in Figure 2.1 and has recently attracted quite some attention, both experimentally and theoretically. It is seen as a prototype system for understanding the dynamics of coupled semiconductor lasers. This is crucial because of the present technological trend of integrating semiconductor lasers on-chip into more complicated optical systems. In particular, coupled lasers are thought to be important devices for use in future all-optical signal processing. Due to the small sizes of semiconductor lasers and the typical distances between the lasers, one is generally dealing with substantial delay in the coupling.

A semiconductor laser on its own behaves simply as a damped oscillator, characterized by its *relaxation oscillation* with a typical frequency in the order of a few GHz; note that this damped oscillation is quite harmonic and should not to be confused with relaxation oscillations in slow-fast systems. However, due to a combination of the material properties of the semiconductor active material and the low reflectivities of the mirrors, this type of laser is very sensitive to external optical influences [17, 19, 29]. For example, it is well-known that delayed optical feedback may destabilize the semiconductor laser. While this is undesirable in applications such as optical data storage, more recently destabilized semiconductor laser systems are being considered and studied as broadband light sources for applications such as private communication [7].

*Afdeling Natuurkunde en Sterrenkunde, Vrije Universiteit Amsterdam, De Boelelaan 1081, 1081 HV Amsterdam, The Netherlands(h.erzgraber@few.vu.nl), Department of Engineering Mathematics, University of Bristol, Bristol BS8 1TR, UK.

†Department of Engineering Mathematics, University of Bristol, Bristol BS8 1TR, UK, Afdeling Natuurkunde en Sterrenkunde, Vrije Universiteit Amsterdam, De Boelelaan 1081, 1081 HV Amsterdam, The Netherlands

‡Afdeling Natuurkunde en Sterrenkunde, Vrije Universiteit Amsterdam, De Boelelaan 1081, 1081 HV Amsterdam, The Netherlands, Research Institute COBRA, Technical University Einhoven, The Netherlands.

The above discussion shows that the semiconductor laser system we consider here can be seen, more generally, as a prototype of two mutually delay-coupled oscillators. There has been quite a lot of interest recently in delay-coupled oscillators in different fields, including chemical oscillations, biological clocks and neural networks; see for example Refs. [33, 32, 25]. On the one hand, delayed coupling of stable subsystems can result in instabilities and even chaos [31]. On the other hand, time delayed coupling can be used to stabilize chaotic systems. Recently studied phenomena in delay-coupled systems include multistabilities, amplitude death or chaos synchronization in conjunction with symmetry breaking [30, 26, 13, 39].

Semiconductor lasers have the advantage that they can be controlled well, so that different dynamics and bifurcations can be studied experimentally. In the setup of Figure 2.1 the coupling is achieved by injecting a part of the emitted light of one laser into the respective other laser. We consider here the case of two SLs which are identical, except for a possible *detuning* between the two lasers. The detuning is the difference in their solitary optical frequencies, that is, the frequency the lasers choose when they are not coupled to each other. Note that SLs can be characterized well and then hand selected, so that the assumption that they have identical material properties can be guaranteed to very good approximation in an experiment. Furthermore, the frequencies of the lasers can be controlled and measured very accurately [1].

Semiconductor laser systems are also very fascinating to study theoretically. They can be modeled well by single-mode rate equations for the electric field E and the inversion N inside the laser cavity. (The inversion is given by the number of electron-hole pairs that can recombine to produce one photon.) External optical influences are modeled by extra terms that lead to a mathematical description in the form of a delay differential equation (DDE), if delay is a feature. Typically, this involves a single fixed delay τ. The best known and most studied laser DDEs are the Lang-Kobayashi equations for a SL subject to optical feedback from a mirror at some fixed distance from the laser [24, 21]. The mutually delay-coupled SLs studied here can also be modeled by rate equations in the same spirit; see Section 2 for details. An important feature of the rate equation model is a number of symmetries, especially a S^1-symmetry of rotation of the electric fields of both lasers.

Since DDEs have an infinite-dimensional phase space, they are a quite difficult class of dynamical systems to study. While linear stability analysis and local bifurcation theory for equilibria of DDEs with fixed delays is well established [2, 11], it is nevertheless quite a challenge to perform a bifurcation analysis of a DDE arising in a specific application. In recent years there has been a substantial development of numerical methods for the bifurcation study of DDEs. Notably, the Matlab package DDE-BIFTOOL allows one to find and follow equilibria and periodic orbits and (some of) their bifurcations. The study of delay effects in SLs is arguably a major motivation and test case for the further development of numerical continuation tool for DDEs [17].

In this paper we make extensive use of numerical continuation to study the basic solutions, called *compound laser modes* (CLMs), of two mutually delay-coupled SLs as modeled by rate equations with a single fixed delay. CLMs are special types of periodic orbits where the motion is only in the direction of the S^1-symmetry. Physically, they correspond to both lasers lasing with constant, but possibly different intensities and at the same optical frequency. We concentrate on the short delay regime, where the coupling time is of the same order of magnitude as the relaxation oscillation period. From the dynamical systems point of view this intermediate regime between ultra

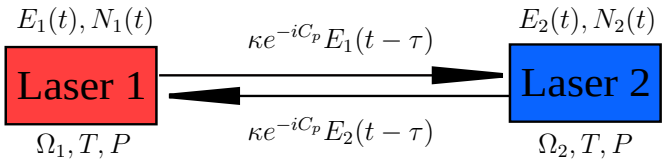

FIG. 2.1. *Sketch of two mutually delay-coupled lasers.*

short delay and long delay times is of particular interest because one can expect rich dynamics due to the competition between the relaxation oscillation frequency and the round-trip frequency. Additionally it has the advantage that the number of CLMs is small, so that their individual behavior can be studied.

More specifically, we present a comprehensive geometric picture of how different types of CLMs coexist, interact and bifurcate in dependence on two main parameters, namely the coupling phase and the detuning between the two lasers. For zero detuning the system has the additional phase-space symmetry of exchanging the two lasers, and we find that certain types of CLMs appear and disappear in pitchfork bifurcations. In fact, the case of zero detuning organizes the bifurcation diagram: when the detuning is 'switched on' the pitchfork bifurcations for zero detuning unfold into saddle-node bifurcations. This results, globally, in branches of CLMs in the form of horseshoes. When the detuning is increased further different branches of CLMs connect, split or disappear in transitions through codimension-one singularities in the surface of CLMs. Finally, a simple limiting situation is reached.

We finish this introduction with a brief overview of the recent literature on the system of two mutually delay-coupled semiconductor lasers. A theoretical study of the system in the limit of zero delay was performed in [40], while the limit for very large delay is the focus of theoretical studies in [16, 36]. Chaos synchronization and symmetry breaking has been reported for long delay times in [13]. An experimental and numerical study of the onset of chaos synchronization for different coupling strengths and injection currents can be found in [23]. In [27] numerical simulations are performed and an analytical formula is derived for the oscillation frequency in the mode beating regime for short delays. Numerical investigations and an approximate thermodynamic potential are the subject of [23, 35]. In [14, 15, 39] it is shown that for a short delay time τ, in the order of the relaxation oscillation period, frequency locking with continuous wave emission and regular intensity oscillations are dominant [14, 15, 39]. A characteristic scenario, consisting of optical frequency locking leading towards successive states of periodic intensity oscillations, as a function of the detuning between the two lasers has recently been demonstrated in [39].

The paper is organized as follows. The rate equation model and its properties are discussed in Section 2. In Section 3 the CLMs are introduced. How CLMs can be continued numerically is explained in Section 4. For the case of zero detuning we derive analytical expressions for the CLMs and present a detailed continuation study. In the following Section 6.1 we consider the effect of small detuning. In Section 6.2 we further increase the detuning, which results in the restructuring of branches of CLMs due to saddle singularities. We discuss the limit of large detuning in Section 6.3. The results are presented in condensed form in Section 6.3 as plots of the surface of CLMs over the two-dimensional parameter space. Finally, Section 7 contains a discussion of avenues for future work.

2. Rate equation model. Our theoretical analysis is based on a set of Lang-Kobayashi-type rate equations for the normalized complex slowly-varying envelope of the optical fields $E_{1,2} = \mathrm{Re}[E_{1,2}] + i\,\mathrm{Im}[E_{1,2}]$ and the normalized inversions $N_{1,2}$. The Lang-Kobayashi equations [21] are an established model to describe a single-mode SL that receives conventional optical feedback. In this situation a part of the emitted light is reflected by a mirror at some fixed distance and is then fed back into the laser. The Lang-Kobayashi equations can be extended for the case of two delay-coupled single mode SL as considered here; for a detailed derivation see [22].

We write the equations in the reference frame of rotation with the averaged optical angular frequency of the two lasers. This means that the optical fields of the lasers are represented by $E_{1,2}(t)e^{i\Omega_0 t}$, where $\Omega_0 = \frac{1}{2}(\Omega_1 + \Omega_2)$ is the average of the lasers' optical angular frequencies $\Omega_{1,2}$, respectively. In non-dimensional form the equations can be written as

$$\frac{dE_1(t)}{dt} = (1+i\alpha)N_1(t)E_1(t) + \kappa e^{-iC_p}E_2(t-\tau) - i\Delta E_1(t)\,, \tag{2.1}$$

$$\frac{dE_2(t)}{dt} = (1+i\alpha)N_2(t)E_2(t) + \kappa e^{-iC_p}E_1(t-\tau) + i\Delta E_2(t)\,, \tag{2.2}$$

$$T\frac{dN_1(t)}{dt} = P - N_1(t) - (1+2N_1(t))|E_1(t)|^2\,, \tag{2.3}$$

$$T\frac{dN_2(t)}{dt} = P - N_2(t) - (1+2N_2(t))|E_2(t)|^2\,. \tag{2.4}$$

In equations (2.1)–(2.4) time t is measured in units of the photon lifetime, which for SL has a typical value on the order of 10 pico seconds. The parameter α is the linewidth enhancement factor. It is typical for SLs and describes the coupling between the phase and the amplitude of the optical fields E. The parameter T is the normalized carrier lifetime T. These are material properties of the laser. The parameter P describes the amount of electrical current used to pump the semiconductor active material. For all parameters we adopt physically meaningful values given in Table 2.1.

Furthermore, the mutual coupling is accounted for by the second term on the right hand-side of (2.1) and (2.2), where τ is the delay time, κ the coupling rate, C_p the coupling phase, and Δ the detuning.

The delay time τ is an intrinsic feature of this coupling, due to the finite propagation time of the light between the spatially separated lasers. We consider here a case of the relatively short distance between the lasers, in the order of centimeters. This is still long compared to the length of the SL cavities of typically a few hundred micrometers. Finally, the coupling rate κ is the fraction of photons coupled into the other laser per unit time.

Our main parameters are the *coupling phase* C_p and the *detuning* Δ. In the reference frame of equations (2.1)–(2.4) C_p depends on the average optical frequency, namely $C_p = \Omega_0\tau$. The parameter Δ measures the difference between the optical frequencies of the two uncoupled lasers with respect to the average frequency, that is, $\Delta = \frac{1}{2}(\Omega_2 - \Omega_1)$. We consider C_p and Δ as independent parameters; this is convenient for the analysis and quite common in the field. The coupling phase C_p can be changed accurately in an experiment by changing the distance between the two lasers on the scale of the optical wavelength, or by exploiting the temperature or pump current dependency of Ω_0 [1]; these changes are so small that the other laser parameters remain unchanged within the experimental accuracy. The detuning Δ

can be changed by increasing Ω_2 and decreasing Ω_1 by the same magnitude, so that the average frequency and, hence, $C_p = \Omega_0\tau$ remains constant. However, it may be more convenient in an experiment to change the optical frequency of only one of the two lasers. For this case equations (2.1)–(2.4) can be rewritten in the frame where one laser has fixed optical frequency [40]. However, then the symmetry of exchanging laser 1 with laser 2 has a more complicated expression.

symbol	laser parameter	value
α	linewidth enhancement factor	2.5
T	electron decay rate	392.0
P	pump parameter	0.23
τ	coupling time	20.0
κ	coupling strength	0.1

TABLE 2.1
Laser parameters and their values.

Equations (2.1)–(2.4) are a system of delay differential equations with a single fixed delay. As such they have an infinite-dimensional phase space, namely the space $C([-\tau, 0], \mathbb{R}^6)$ of continuous functions over the delay interval $[-\tau, 0]$ with values in (E_1, E_2, N_1, N_2)-space. Thus, in contrast to ordinary differential equations, a single initial condition $x_0 \in \mathbb{R}^6$ is not enough to determine the future evolution of the system. Indeed it is required to prescribe initial data on the entire interval $[-\tau, 0]$. We refer to [2, 11] as general references on delay equations; see also [9] for a background section on DDEs in the context of a SL with delayed feedback.

Crucial for what follows are a number of symmetries of equations (2.1)–(2.4). First of all, there is the continuous S^1-symmetry

$$(E_1, E_2, N_1, N_2) \to (E_1 e^{ib}, E_2 e^{ib}, N_1, N_2)\,. \tag{2.5}$$

This phase-space symmetry is a typical feature of Lang-Kobayashi-type equations, provided that no phase conjugation is involved [20]. Any solution of equations (2.1)–(2.4) is invariant under any phase shift of both electric fields E_1 and E_2. The S^1-symmetry motivates the ansatz (3.1)–(3.4) of the compound laser modes (CLMs) of Section 3 with a common frequency for both lasers.

Secondly, there is the reflection symmetry

$$(E_1, E_2, N_1, N_2, \Delta) \to (E_2, E_1, N_2, N_1, -\Delta) \tag{2.6}$$

of interchanging the two lasers, which results in a sign change of Δ. For zero detuning, that is, for $\Delta = 0.0$, this symmetry is a $\mathbb{Z}_2$-symmetry in phase space. When the detuning Δ is then 'switched on' this phase-space symmetry is broken, which has important consequences for the organization of the CLMs; see section 6.1.

Thirdly, there is the 2π-translational symmetry

$$(E_1, E_2, N_1, N_2, C_p) \to (E_1, E_2, N_1, N_2, C_p + 2\pi)\,, \tag{2.7}$$

in the feedback phase C_p-space. As a consequence, the parameter C_p is a circle. We refer to this symmetry as the 2π-translational symmetry. It is often useful to show bifurcation diagrams in the covering space $\mathbb{R}$ of the circle, that is, over several fundamental domains (of length 2π) of the symmetry (2.7).

Fourthly, there is the symmetry

$$(E_1, E_2, N_1, N_2, C_p) \to (E_1, -E_2, N_1, N_2, C_p + \pi)\,, \tag{2.8}$$

which is a π-translational symmetry in the feedback phase C_p, combined with a sign change in the optical field of one laser, say, E_2. Due to the S^1-symmetry (2.5) one could also change the sign of E_1. We refer to this symmetry as the π-translational symmetry. As we will see in Section 5, it provides a link between different types of CLMs.

3. Coupled laser modes. The basic solutions of equations (2.1)–(2.4) are called the *coupled laser modes* (CLMs); they are of the form

$$E_1(t) = R_1^s e^{i\omega^s t}\,, \tag{3.1}$$

$$E_2(t) = R_2^s e^{i\omega^s t + i\sigma}\,, \tag{3.2}$$

$$N_1(t) = N_1^s\,, \tag{3.3}$$

$$N_2(t) = N_2^s\,, \tag{3.4}$$

where R_i^s, N_i^s, ω^s, and σ are time independent and real valued. Additionally, R_i^s are taken to be positive without loss of generality. We allow different amplitudes R_i^s and different steady state inversions N_i^s. However, the lasers must have the same frequency ω^s, which is implied by the S^1-symmetry (2.5). Here ω^s is the deviation between the average solitary laser frequency Ω_0 and the frequency of the coupled laser system. There may also be some time-independent phase shift σ between the lasers. Mathematically, CLMs are periodic orbits, with frequencies that depend on other parameters, where the rotation is in the direction of the symmetry group only. This property of the CLMs must be taken into account when one wants to continue them numerically; see Section 4. Physically, CLMs are frequency locked states, in which the lasers operate with constant, but possibly different intensities.

Note that we consider here the situation that the pump current is sufficiently large, so that the overall system is in the 'on-state', that is the optical fields have non-zero amplitude. Mathematically, this means that the 'off-state' given by $(E_1, E_2, N_1, N_2) = (0, 0, P, P)$ is unstable.

Inserting ansatz (3.1)–(3.4) into (2.1)–(2.4) gives the set of six coupled nonlinear transcendental equations for the six unknowns:

$$0 = R_1^s N_1^s + \kappa R_2^s \cos(-C_p - \omega^s \tau + \sigma)\,, \tag{3.5}$$

$$(\omega^s + \Delta) = \alpha N_1^s + \kappa \frac{R_2^s}{R_1^s} \sin(-C_p - \omega^s \tau + \sigma)\,, \tag{3.6}$$

$$0 = R_2^s N_2^s + \kappa R_1^s \cos(-C_p - \omega^s \tau - \sigma)\,, \tag{3.7}$$

$$(\omega^s - \Delta) = \alpha N_2^s + \kappa \frac{R_1^s}{R_2^s} \sin(-C_p - \omega^s \tau - \sigma)\,, \tag{3.8}$$

$$0 = P - N_1^s - (1 + 2N_1^s)|R_1^s|^2\,, \tag{3.9}$$

$$0 = P - N_2^s - (1 + 2N_2^s)|R_2^s|^2\,. \tag{3.10}$$

There is no obvious analytical strategy for solving for the unknowns in some closed form that allows one to create an overall picture of how the CLMs depend on parameters, for example, on C_p and Δ. In fact, the situation is a lot more complicated than for the case of the Lang-Kobayashi equations of a semiconductor laser with feedback, for which a partial analytical picture is now emerging [28]. It is of course possible

to find individual solutions of (3.5)–(3.10) numerically, for example, by root solving with Newton's method. Such roots can then be followed in relevant parameters with standard continuation software, such as AUTO [3].

The approach we take here is in this spirit, but we find and follow CLMs in the full DDE (2.1)–(2.4) by using the package DDE-BIFTOOL [4]. This has the advantage that we obtain stability information along branches of CLMs; see Section 4 for details of the numerical procedure.

Furthermore, we gain insight into special cases of CLMs by a study of some special cases of (3.5)–(3.10). Of special interest is the relationship between the frequency ω^s and the phase difference σ. We eliminate the unknown variables R_1, R_2, N_1, N_2 from (3.5)–(3.8), which results in the transcendental equation

$$\begin{aligned}(\omega^s)^2 = \kappa^2(1+\alpha^2)[&\sin(C_p + \omega^s\tau + \sigma + \arctan(\alpha)) \\ &\times \sin(C_p + \omega^s\tau - \sigma + \arctan(\alpha))] - \Delta^2\,.\end{aligned} \tag{3.11}$$

As we will see in Section 5, this equation allows us to identify certain CLMs as solutions of an associated Lang-Kobayashi equation for a laser with optical feedback.

4. Continuation of CLMs. The package DDE-BIFTOOL provides Matlab routines for the numerical continuation analysis of DDEs [4]. From a starting solution, such as a steady state or a periodic orbit, DDE-BIFTOOL is able to follow a solution branch in one parameter. Furthermore, stability information in the form of eigenvalues or Floquet multipliers can be computed along the branch. In this way, local codimension-one bifurcations can be detected; some of them can be followed in two parameters.

In order to use DDE-BIFTOOL to follow branches of CLMs in (2.1)–(2.4) one needs to realize that CLMs are periodic orbits. However, CLMs are special types of periodic orbits: $R^s_{1,2}$ and $N^s_{1,2}$ are constant, so that the periodic motion is purely in the direction of the continuous S^1-symmetry, with constant speed ω^s and a time-independent phase difference σ; one also speaks of CLMs as group orbits of the S^1-symmetry. The situation is conceptually the same as that for the external cavity modes (ECMs) of the Lang-Kobayashi equations [20, 10].

We can exploit the special nature of the CLMs to continue them as equilibria with DDE-BIFTOOL of an appropriately amended equation; see also [10, 18]. The idea is to move into the frame that is rotating with the speed given by the unknown frequency ω_s. (Recall that ω_s is different for different CLMs, so that the S^1-symmetry cannot be divided out globally [20].) In order to use DDE-BIFTOOL this can be done by introducing the new parameter b, replacing $E_{1,2}(t)$ in equations (2.1) and (2.2) with

$$E_{1,2}(t)e^{ibt}\,. \tag{4.1}$$

This gives the new equations

$$\frac{dE_1}{dt} = (1+i\alpha)N_1E_1 + \kappa e^{-iC_p}E_2(t-\tau) - i(b+\Delta)E_1\,, \tag{4.2}$$

$$\frac{dE_2}{dt} = (1+i\alpha)N_2E_2 + \kappa e^{-iC_p}E_1(t-\tau) - i(b-\Delta)E_2\,, \tag{4.3}$$

while equations(2.3) and (2.4) remain unchanged. During the continuation b is an additional free parameter that is then fixed to $b = \omega^s$, so that the respective CLM is now an equilibrium of equations (4.2),(4.3), (2.3), and (2.4). Because of the S^1-symmetry, the CLM gives rise to a whole family of non-isolated equilibria in this

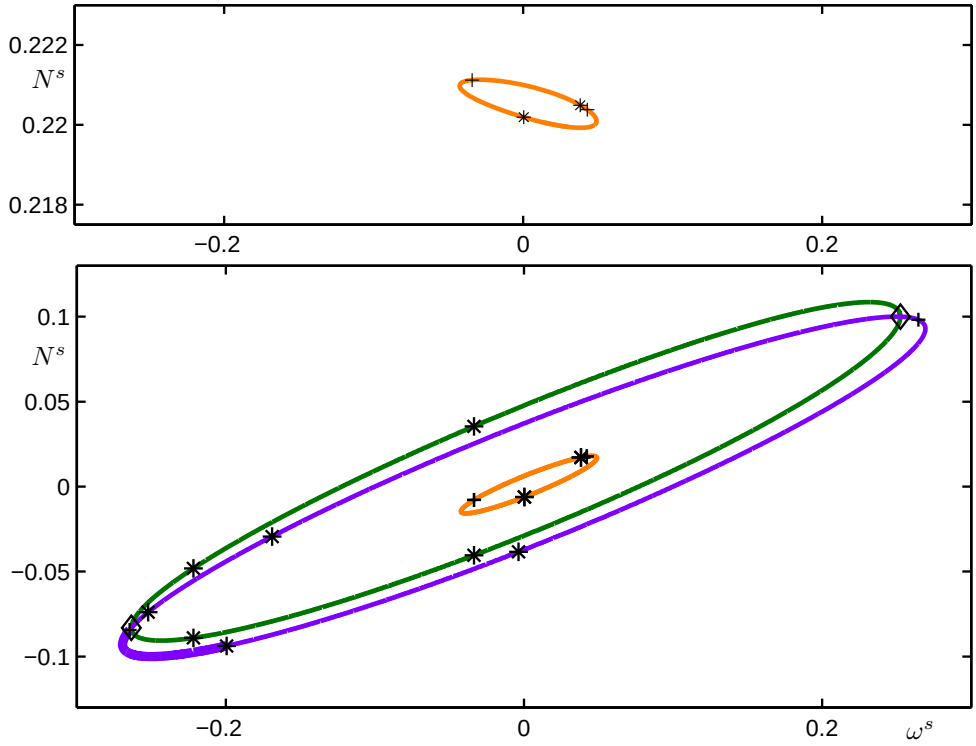

FIG. 5.1. *Curves of CLMs for zero detuning in the (ω^s, N^s)-plane. For the constant-phase CLMs (purple curve) the inversions of both lasers are identical, while for the bifurcating intermediate-phase CLMs (green curve) they are different. There is another disconnected branch of CLMs (orange curves), where the inversion of the two lasers are on two different curves, one for larger values of N^s. (Note the different scale of the vertical axis.) Throughout the paper saddle-node bifurcations are marked by pluses (+), Hopf bifurcations by stars (∗) and pitchfork bifurcations by diamonds (◇); stable regions are plotted as bold curves. Note that saddle-node bifurcations do not coincide with folds with respect to ω^s.*

setup. To obtain an isolated solution one needs to fix the phase, which can be done, for example, by requiring that $\mathrm{Im}(E_1) = 0$.

Along a branch of CLMs stability information is computed using DDE-BIFTOOL in the usual way but with one exception: there is always one extra zero-eigenvalue due to direction of group action, which is neutral. Thus, we can detect codimension-one bifurcations as for any equilibrium, namely saddle-node bifurcations, pitchfork bifurcations and Hopf bifurcations. For the interpretation of the results it is important to keep in mind that we are actually dealing with bifurcations of CLMs, which are group orbits of the S^1-symmetry of the respective equilibria. While saddle-node and pitchfork bifurcations simply lead to the creation of different branches of CLMs, Hopf bifurcations actually lead to bifurcating tori in phase space.

In what follows we use DDE-BIFTOOL to derive a comprehensive pictures of the CLMs, including stability information, in dependence on the feedback phase C_p and the detuning Δ. To this end, we first consider the case of zero detuning in Section 5 and then the influence of nonzero detuning in Section 6.

5. CLMs for Zero Detuning. For zero detuning, $\Delta = 0$, the two lasers would operate with the same solitary optical frequency. While the detuning is experimentally

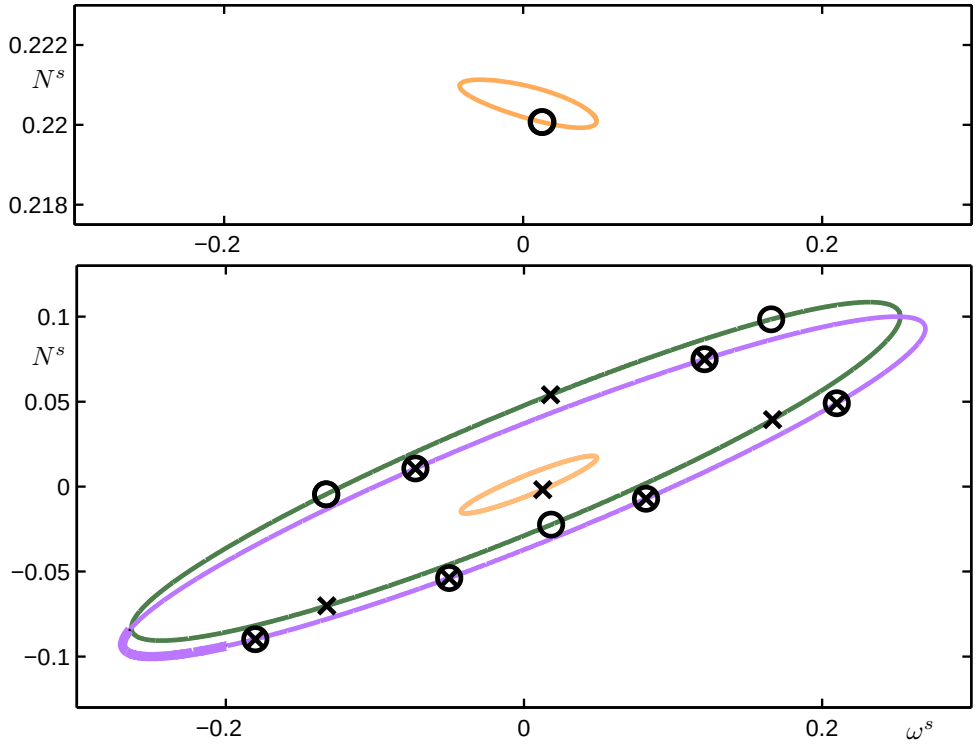

FIG. 5.2. *The curves of CLMs for zero detuning in the (ω^s, N^s)-plane as in Figure 5.1, but with CLMs for $C_p = 0$. Crosses ($\times$) mark the inversion of laser 1 and circles ($\circ$) that of laser 2. A second set of solutions, with crosses and circles interchanged, exists as a result of the second reflection symmetry (2.6). See also the accompanying animation ekl_a1.gif.*

easily accessible and can be controlled with good accuracy [12], one may argue that $\Delta = 0$ is not attainable exactly in an experiment. However, it turns out that this special case organizes the dynamics even for small nonzero detuning.

For $\Delta = 0$ the symmetry (2.6) of exchanging the two lasers is a reflectional symmetry in phase space. In particular, equation (3.11) reduces to

$$(\omega^s)^2 = \kappa^2(1+\alpha^2)[\sin(C_p + \omega^s\tau + \sigma + \arctan(\alpha)) \times \sin(C_p + \omega^s\tau - \sigma + \arctan(\alpha))]\,. \tag{5.1}$$

For the special choices $\sigma = 0$ and $\sigma = \pi$ we obtain

$$\omega^s = \mp\kappa\sqrt{1+\alpha^2}\,\sin(C_p + \omega^s\tau \arctan(\alpha)) \tag{5.2}$$

with the respective choice of $\mp$.

We call solutions of (5.2) the *constant-phase CLMs*, where we distinguish further between *in-phase CLMs* with $\sigma = 0$ and *anti-phase CLMs* with $\sigma = \pi$. Equation (5.2) is in fact the determining equation for the ECMs of the Lang-Kobayashi equations describing a laser with conventional optical feedback from a mirror at half the distance between the two lasers, except for the allowing for both signs $\mp$. As an immediate consequence, the constant-phase CLMs lie on an ellipse in the (ω^s, N^s)-plane. In particular, for constant-phase CLMs one has $R_1^s = R_2^s$ and $N_1^s = N_2^s$, which means

that both lasers operate with the same intensity. In-phase CLMs have zero phase difference, $\sigma = 0$, and are described by (5.2) with a minus sign. Physically, this is the case of constructive interference between the optical fields of the two lasers. On the other hand, for anti-phase CLM with a phase difference of $\sigma = \pi$, there is destructive interference between the optical fields of the two lasers, as is expressed by the plus sign in (5.2). Mathematically, the in-phase CLMs are related to the anti-phase CLMs by the π-translational symmetry (2.8).

The constant-phase CLMs are the most obvious solutions of Equations (3.5)–(3.10) for zero detuning. However, a bifurcation analysis with numerical continuation shows that even for zero detuning there are additional CLMs where σ is not constant, but some function of C_p. We call these solutions *intermediate-phase* CLMs. For this type of CLMs one finds that $R_1^s \neq R_2^s$ and $N_1^s \neq N_2^s$, which means that the two lasers operate with different intensities.

Figure 5.1 shows curves of CLMs in the (ω^s, N^s)-plane. The projection is the representation of choice in the physics literature (also for the Lang-Kobayashi equations) because in effect, it 'hides' the 2π-translational symmetry of the parameter C_p. All CLMs lie on closed curves. Furthermore, the frequency ω^s is a quantity that can be measured in an experiment and N^s is directly related to the laser intensity. Each curve is parameterized by the feedback phase C_p, meaning that it represents all CLMs of a given type that exist for any choice of C_p. The symbols in Figure 5.1 indicate points where saddle-node, pitchfork and Hopf bifurcations take place along the different branches as C_p is changed. The constant-phase CLMs form the purple ellipse. The bifurcating intermediate-phase CLMs lie on the green closed curve which also has the shape of an ellipse for our choice of parameters. Additionally, there is a separate branch of intermediate-phase CLMs, namely the two orange islands. For a given C_p, there is a fixed number of CLMs, which lie on the respective curves. This is illustrated in Figure 5.2 for $C_p = 0$, where circles ($\circ$) mark the inversion of laser 1 and crosses ($\times$) the inversion of laser 2. There is a second set of solutions due to the reflection symmetry (2.6), which can be obtained by interchanging crosses ($\times$) with circles ($\circ$).

We now describe how the different types of CLMs move over the respective curves as C_p is decreased; compare Figures 5.1 and 5.2 and the accompanying animation ekl_a1.gif. Constant-phase CLMs move over the purple ellipse. In-phase CLMs and anti-phase CLMs are born in pairs in the saddle-node bifurcation in the low-inversion region. The saddle-node bifurcations are close to the folds with respect to ω^s, but they do not take place exactly at the folds because ω^s is not a bifurcation parameter. When C_p is decreased, the saddle is moving on the upper half and the node is moving on the lower half of the purple ellipse towards the high-inversion region. Eventually they coalesce and disappear in the second saddle-node bifurcation in the high-inversion region. Along the way, the constant-phase CLMs change their stability several times, mostly in Hopf bifurcations. The constant-phase CLMs in the boldfaced region of the purple ellipse are stable. In this region the two lasers show stable emission with the same intensity and, depending on the exact range of C_p, a phase difference of either zero or π. This stable region is bounded by a saddle-node bifurcation on the left and by a Hopf bifurcation on the right.

The pitchfork bifurcation is responsible for the creation of a pair of intermediate-phase CLMs, which lie on the green ellipse in Figures 5.1 and 5.2. For intermediate-phase CLMs $N_1^s \neq N_2^s$. In fact, the inversion of, say, laser 1 can be found on the lower half of the green ellipse, whereas the inversion of laser 2 is on the upper half;

due to symmetry there is a second solution with laser 1 and laser 2 exchanged. For decreasing C_p, the intermediate-phase CLMs travel along their ellipse from the low-inversion region towards the high-inversion region, where they coalesce and disappear in the second pitchfork bifurcation. We can distinguish between intermediate-phase CLMs that are born in a pitchfork bifurcation of an in-phase CLMs and intermediate CLMs that a born in a pitchfork bifurcation of an anti-phase CLM, which we call *increasing-phase CLMs* and *decreasing-phase CLMs*, respectively.

Finally, there is the set of intermediate-phase CLMs on the separate orange islands. Being intermediate-phase CLMs, they also have non-identical inversions, $N_1^s \neq N_2^s$, and non-identical amplitudes, $R_1^s \neq R_2^s$. The inversion of, say, laser 1 takes values around its solitary value; corresponding to the origin in Figures 5.1 and 5.2, whereas the inversion of laser 2 has significantly higher values of the inversion, as can be seen in the upper panels of these figures. Again due to symmetry there is a second solution with laser 1 and laser 2 exchanged. When decreasing C_p, these intermediate-phase CLMs are born in pairs in a saddle-node bifurcation on the left side of the curve, that is for negative ω^s. Then they move along the orange, ellipse-like curves, one on the upper ellipse and the other one on the lower ellipse, and eventually coalesce and disappear in the second saddle-node bifurcation.

A disadvantage of the projection from the bifurcation theory point of view is that neither N^s nor ω^s are a bifurcation parameters, so that Figure 5.1 is not a bifurcation diagram. In particular, we already mentioned that the saddle-node bifurcations do not coincide with the folds with respect to ω^s. Therefore, we now study the CLMs as a function of C_p, which is a main bifurcation parameter we consider here. To this end, we show in Figures 5.3–5.4 different curves of CLMs as a function of C_p. This representation makes all the symmetries explicit and allows us to discuss in detail how the different types of CLMs depend on the bifurcation parameter C_p and how they interact. The number and location of CLMs for a given C_p can simply be read off by considering all intersections of curves of CLMs with a vertical line corresponding to the value of C_p; for example, the CLMs in Figure 5.2 correspond to the intersection with the line $\{C_p = 0\}$; in this projection the saddle-node bifurcations are the folds with respect to C_p. It is convenient to show the respective curves of CLMs over several multiples of 2π, meaning that we consider several fundamental domains of the 2π-translational symmetry (2.7).

In Figure 5.3 we show the constant-phase and bifurcating intermediate-phase CLMs in the (C_p, N^s)-plane. Panel (a) shows the constant-phase CLMs, namely the in-phase CLMs in pink and the anti-phase CLMs in purple. Both form a single, self-intersecting curve, and the image is indeed 2π-translationally invariant. A translation by π transforms the pink into the purple curve and vice versa, which represents the relation between the in-phase and the anti-phase CLMs as given by (2.8). Panel (b) of Figure 5.3 shows the intermediate-phase CLMs that bifurcate in the pitchfork bifurcations from the constant-phase CLMs, where the increasing-phase CLMs are shown in light green and the decreasing-phase CLMs in dark green. There are infinitely many closed curves that appear to have the shape of an ellipse. The image is again invariant under a translation by 2π, while a translation by π transforms the light green into the dark green curves, that is, increasing-phase into decreasing-phase CLMs.

Figure 5.4 illustrates how the constant-phase and the bifurcating intermediate-phase CLMs interact when seen as a function of C_p. Panel (a) simply shows both sets of curves plotted together in the (C_p, N^s)-plane. The intersections of curves marked by a diamond ($\diamond$) are the pitchfork bifurcations; all other intersections are

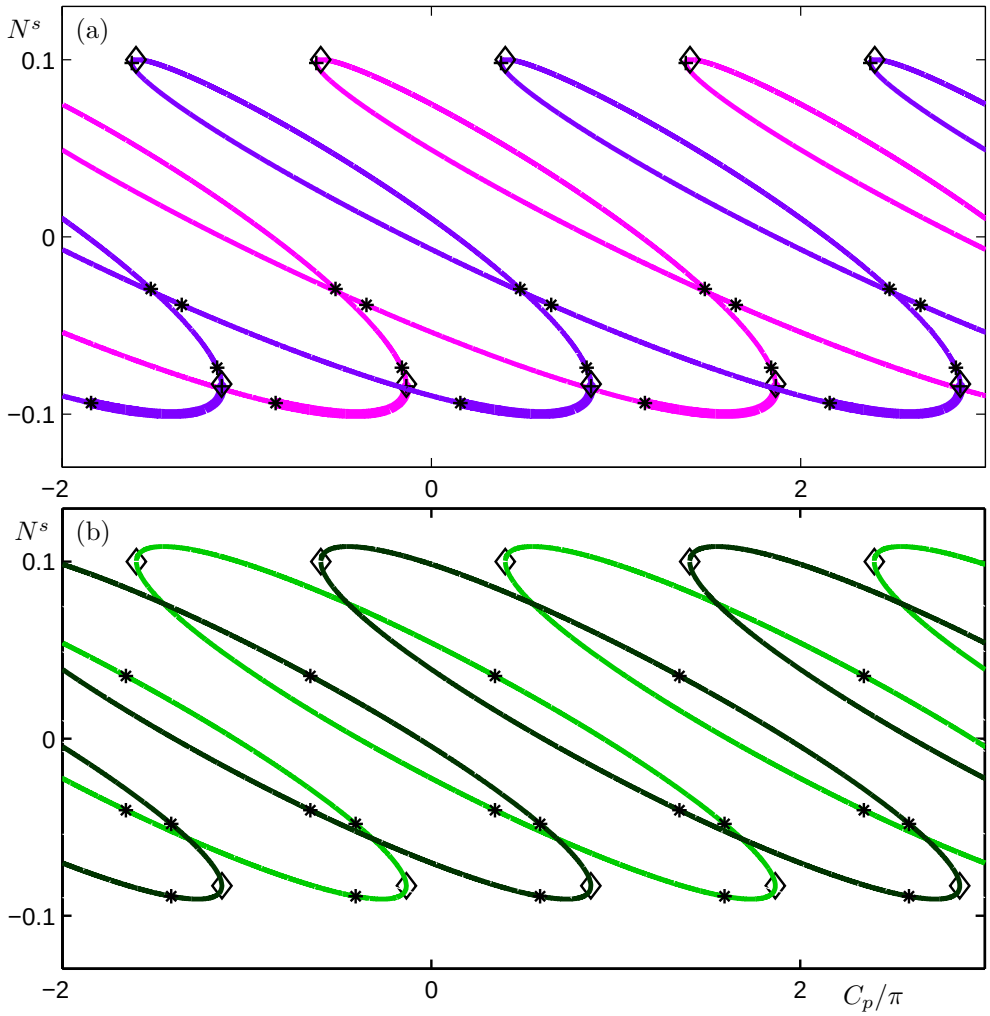

FIG. 5.3. *CLMs for zero detuning from Figure 5.1 plotted in the (C_p, N^s)-plane. The constant-phase CLMs form two infinite long self-intersecting curves (a). The in-phase CLMs (pink curve) and the anti-phase CLMs (purple curve) that are each other's image under the π-translational symmetry (2.8). The intermediate-phase CLMs, on the other hand, form infinitely many closed curves(b). The increasing-phase CLMs (light green curves) and the decreasing-phase CLMs (dark green curves) are each other's image under the π-translational symmetry (2.8).*

due to projection. This image clearly shows how the infinitely many ellipse-like curves of intermediate-phase CLMs provide the connection between the two single curves of constant-phase CLMs. This point is further brought out in panel (b) of Figure 5.4, where we show the same CLMs in the (C_p, σ)-plane; notice the additional 2π-symmetry of the figure in the phase difference σ. In this representation the constant-phase CLMs trace out a straight line at $\sigma = 0$ for the in-phase CLMs and at $\sigma = \pm\pi$ for the anti-phase CLMs. The different ellipse-like curves of intermediate-phase CLMs in Figures 5.3, on the other hand, lead to an intriguing array of additional curves in the (C_p, σ)-plane. Let us concentrate on the right most dark green curve with a pitchfork bifurcation of an in-phase CLM at $(C_p, \sigma) \approx (2.8\pi, 0)$. For decreasing

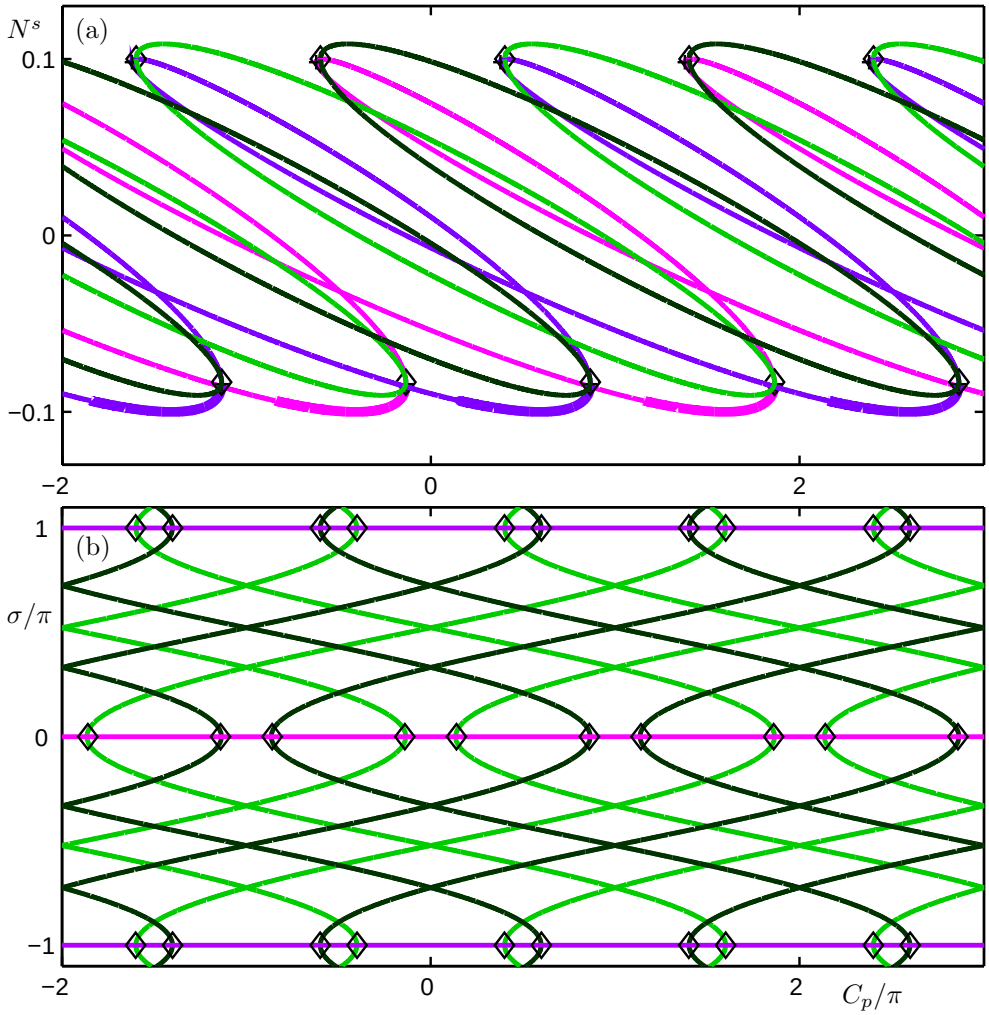

FIG. 5.4. *The constant-phase CLMs and the bifurcating intermediate-phase CLMs from Figure 5.2 plotted together in the (C_p, N^s)-plane (a) and in the (C_p, σ)-plane (b). The intersections marked by diamonds ($\diamond$) are the pitchfork bifurcations.*

C_p, two branches emerge from this point, one is going upwards towards higher σ, the other is going downwards towards lower σ. While C_p decreases, the two intermediate-phase CLMs gain an additional phase shift of $\pm\pi$. Eventually they both intersect with the branch of anti-phase CLMs at around $(C_p, \sigma) = (-0.5\pi, \pm\pi)$. This is the point of the second pitchfork bifurcation, where this particular pair of intermediate-phase CLMs disappears. Due to the 2π-symmetry in σ the anti-phase CLMs at $\sigma = -\pi$ is identical to the one at $\sigma = \pi$. All other green branches connect in-phase and anti-phase CLMs in a similar way. The relationship between light green and dark green branches is again given by the symmetry (2.8), which in the (C_p, σ)-plane is given by $(C_p, \sigma) \to (C_p + \pi, \sigma + \pi)$.

We end this section by considering in Figure 5.5 the other intermediate-phase CLMs corresponding to the orange curve in Figure 5.1. Panels (a) and (b) shows these CLMs in the (C_p, N^s)-plane. Since the inversions of the two lasers are very

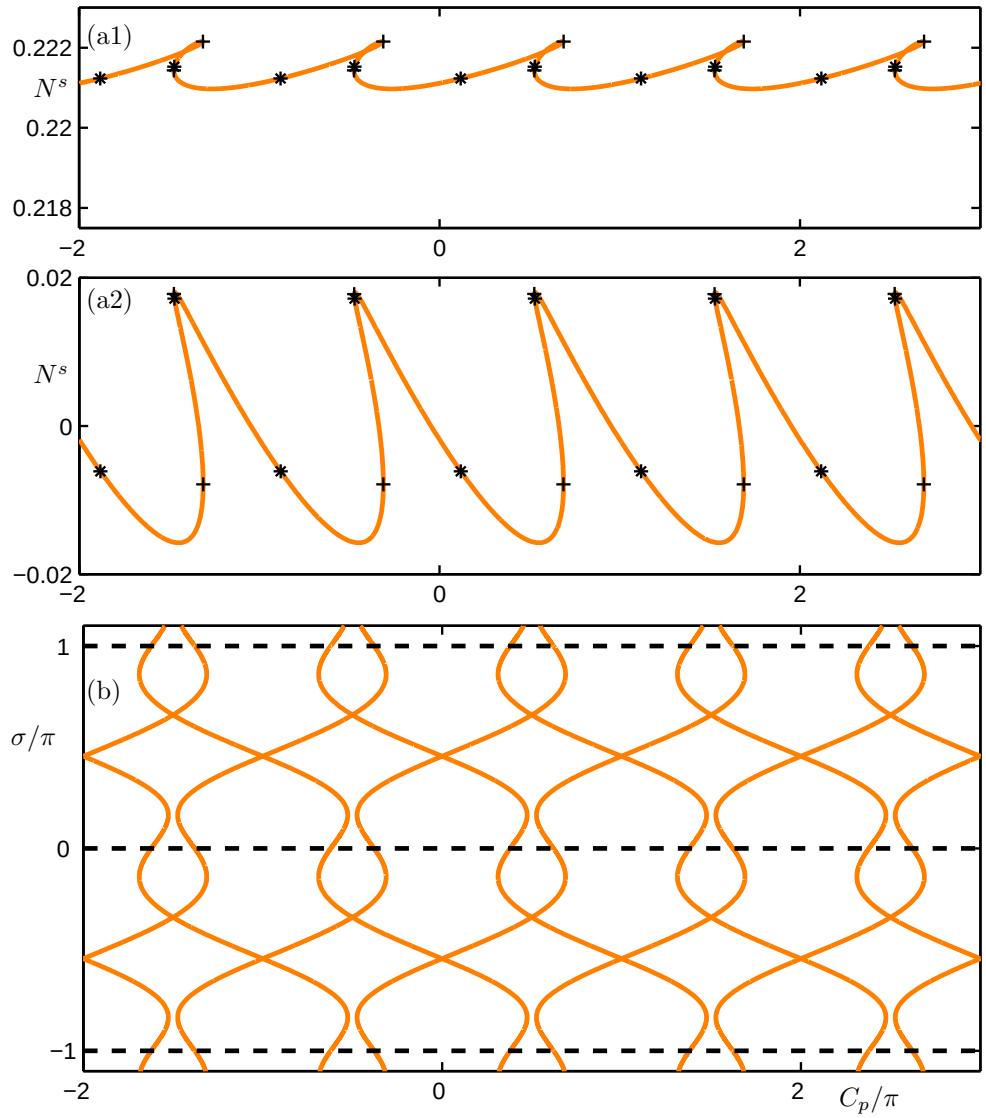

FIG. 5.5. *The other intermediate-phase CLMs from Figure 5.1 plotted in the* (C_p, N^s)*-plane for one laser (a1), the other laser (a2), and in the* (C_p, σ)*-plane (b).*

different we plot them in different panels; note also the difference in the vertical scales. These intermediate-phase CLMs trace out two curves, one for N^s around zero and one for N^s around 0.222. The image in Figure 5.5 is not only invariant under translation by 2π but also under translation by π. This means that for this type of intermediate-phase CLMs one cannot distinguish two different types that are each others counterparts under exchanging laser 1 and laser 2. Panel (c) of Figure 5.5 shows the phase difference σ of these intermediate-phase CLMs, which are born in pairs in saddle-node bifurcations, corresponding to folds of the branches. The different orange curves are each others image under the symmetries (2.8) and (2.7), which in the (C_p, σ)-plane are given by $(C_p, \sigma) \to (C_p + \pi, \sigma + \pi)$ and $(C_p, \sigma) \to (C_p + 2\pi, \sigma + 2\pi)$,

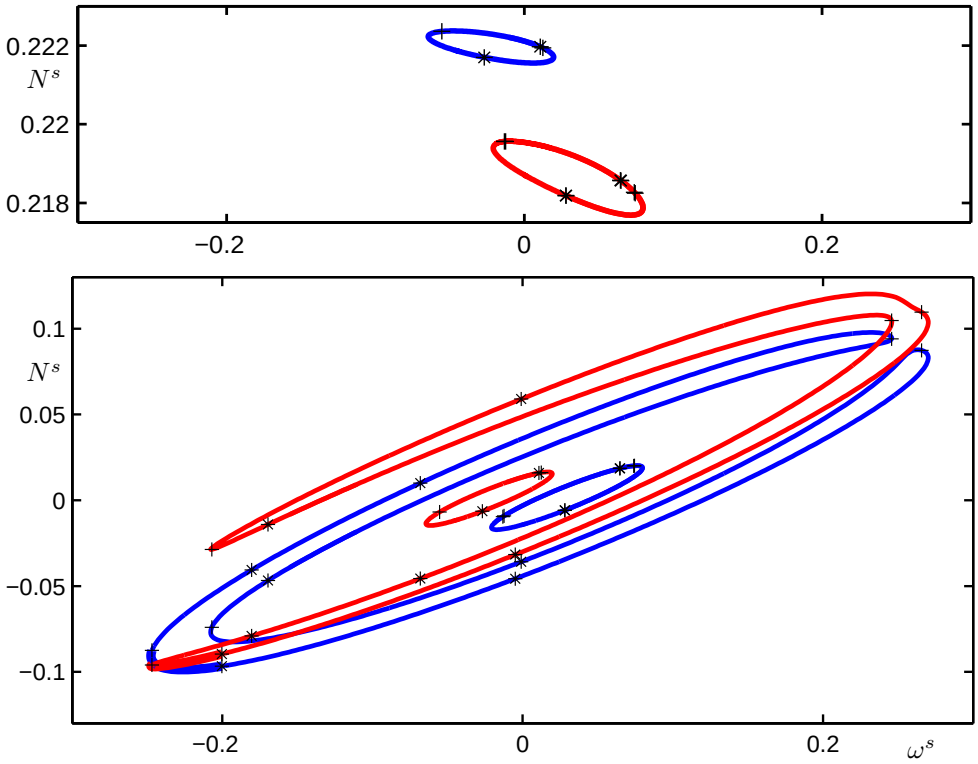

FIG. 6.1. *CLMs for $\Delta = 0.025$ in the (ω^s, N^s)-plane, where we distinguish between the red detuned laser 1 (red curves) and the blue detuned laser 2 (blue curves).*

respectively. Note that, in contrast to the other type of intermediate-phase CLMs in Figure 5.4, these intermediate-phase CLMs do not remain in an finite interval of C_p values. Instead, as a function of C_p they continuously gain (or lose) in phase difference σ.

6. CLMs for Nonzero Detuning. In this section we study in detail how the structure of the CLMs discussed in the last section changes with the detuning. Due to the symmetry (2.6), we may restrict our attention to $\Delta > 0$. We first consider in Section 6.1 the case of relatively small Δ, which can be seen as being 'organized' by the CLMs for zero detuning. Indeed $\Delta \neq 0$ breaks the phase space symmetry of exchanging the two lasers. As a result, the pitchfork bifurcations for $\Delta = 0$ unfold to saddle-node bifurcations leading to an interesting global organization of the different branches of CLMs. In fact, locally small detuning has only little effect and to some extent one still can speak of identical lasers. In Section 6.2 we show that for intermediate Δ there are further interactions between different branches of CLMs due to transitions through saddles and extrema of the surface of CLMs in the three-dimensional (C_p, Δ, N^s)-space. Finally, we consider the limit of very large Δ in Section 6.3.

6.1. Perturbation from Zero Detuning. As an entry point to the analysis of the CLMs for nonzero detuning we present in Figure 6.1 again the 'physical representation' of the CLMs in the (ω^s, N^s)-plane. The colors now refer to the two different

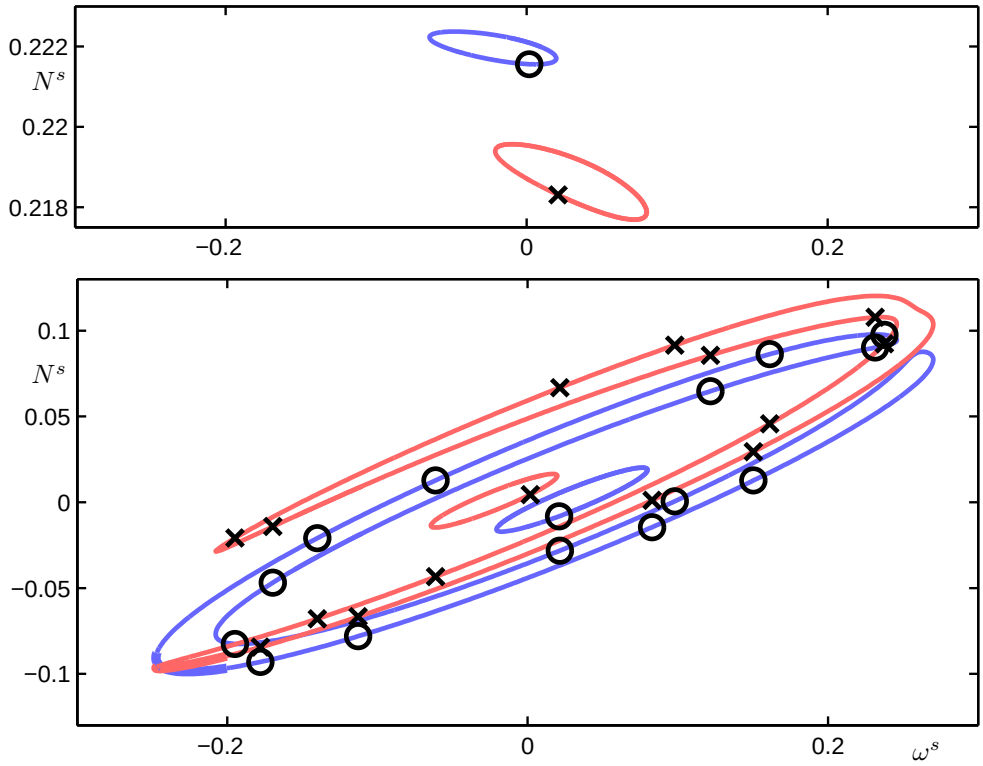

FIG. 6.2. *CLMs for* $\Delta = 0.025$ *in the* (ω^s, N^s)*-plane for fixed value of* $C_p = 0$*. Crosses* $(\times)$ *mark the inversion of laser 1 and circles* $(\circ)$ *that of laser 2. See also the accompanying animation ekl_a2.gif.*

lasers: red corresponds to laser 1, which is 'red detuned' with respect to the average optical frequency, and blue corresponds to laser 2, which is 'blue detuned' with respect to the average optical frequency. Recall that Equations (2.1)–(2.4) are written in the reference frame of average optical frequency $\frac{1}{2}(\Omega_1 + \Omega_2)$; the system can be detuned without changing the coupling phase C_p.

For nonzero detuning the inversions of the lasers are no longer identical, that is, $N_1^s \neq N_2^s$. Thus, different curves can be seen for laser 1 and laser 2, respectively. We first concentrate on the two large closed curves in the shape of horseshoes. Their structure can be understood by the unfolding of the pitchfork bifurcations for zero detuning. Depending on the sign of the unfolding parameter, there are two generic possibilities of locally unfolding a pitchfork bifurcation, each consisting of a saddle-node bifurcation and a separated branch [33]. In the coupled laser system both possibilities exist, one in the low-inversion region and one in the high-inversion region. Globally, for the chosen set of parameters, the unfolding of the pitchfork bifurcations leads to the formation of the red and the blue horseshoes.

Furthermore, the small ellipses originate from the two separate ellipses of intermediate-phase CLMs for zero detuning. Each of them is now split up into a red and a blue ellipse. A single CLM for fixed C_p now corresponds to one point on a red curve and another point on the blue curve. This is illustrated in Figure 6.2 for $C_p = 0$, where circles $(\circ)$ mark the inversion of the red laser 1 and crosses $(\times)$ that of the blue laser 2.

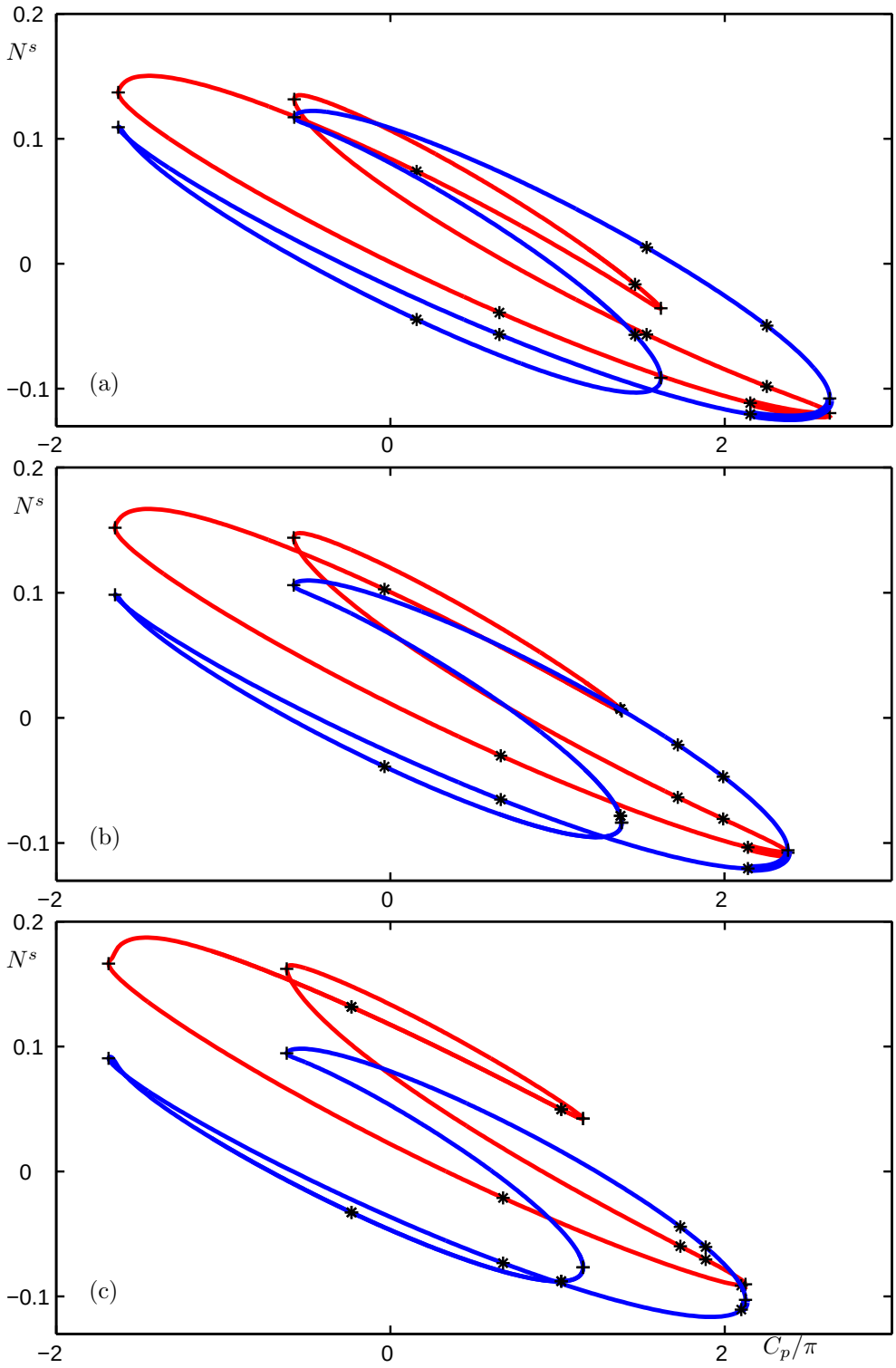

FIG. 6.3. *Detuning sequence of CLMs in the* (C_p, N^s)*-plane. Panel (a) shows the CLMs for* $\Delta = 0.025$ *from Figure 5.1, while in panel (b) and (c)* Δ *takes the values* 0.05 *and* 0.075*, respectively. See also the accompanying animations ekl_a3.gif and ekl_a4.gif in the* (ω^s, N^s)*-plane.*

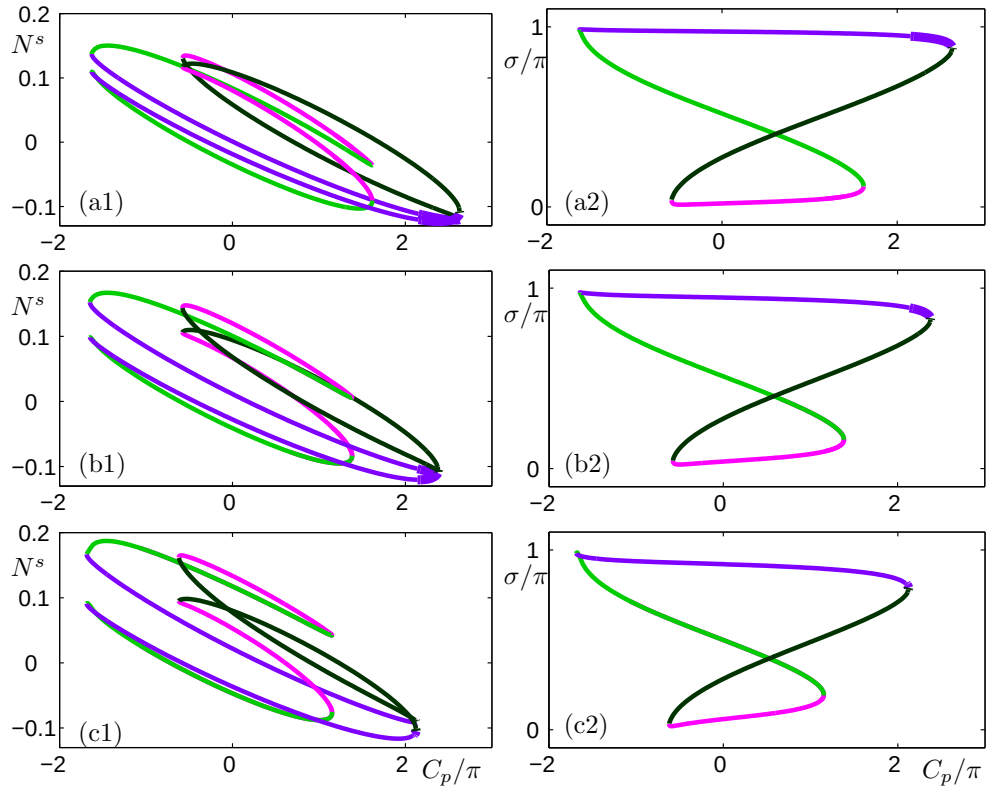

FIG. 6.4. *The detuning sequence in the (C_p, N^s)-plane from Figure 6.3 shown in the (C_p, N^s)-plane (left column) and in the (C_p, σ)-plane (right column). The different branches are color coded as in Figure 5.4 to identify (approximate) in-phase, anti-phase, increasing-phase, and decreasing-phase CLMs.*

When C_p is decreased, CLMs move over the different pairs of red and blue branches; compare Figures 6.1 and 6.2 and the accompanying animation ekl_a2.gif. CLMs are formed in saddle-node bifurcations in the low-inversion region, travel along the horseshoes and then disappear in the high-inversion region in another saddle-node bifurcation. Similarly, for the separate ellipses the associated CLMs are formed in saddle-node bifurcations on the low frequency side of the respective ellipse and disappear in saddle-node bifurcations on the high frequency side. Again, a CLM for fixed C_p corresponds to one point on a red curve and one on the corresponding blue curve.

The connection with the case of zero detuning is obviously given by decreasing Δ back to zero. Then the two horseshoes move closer and closer together and in the limit form the two ellipses of the constant-phase and bifurcating intermediate-phase CLMs. Similarly, the ellipses of separate intermediate-phase CLMs move together and then form only two ellipses; compare Figures 6.1 and Figure 5.1 and see the accompanying animation ekl_a2.gif .

We now consider the CLMs for (small) nonzero detuning in dependence of the parameter C_p, that is, in the (C_p, N^s)-plane. Figure 6.3 shows the curves that correspond to the red and blue horseshoes for three different values of increasing Δ; panel (a) is actually for the data in Figure 6.1. Both the curve for the red and that for

the blue laser are closed curves with a single self-intersection. Note that we only plot one such curve each; there are, in fact, infinitely many copies due to the translational symmetries (2.8) and (2.7). As the detuning is increased, the curve of the red and the blue laser move further apart, but the structure of the branches remains topologically the same in Figure 6.3.

Figure 6.4 shows the curves of CLMs of Figure 6.3 in the (C_p, N^s)-plane (left column) and the (C_p, σ)-plane (right column), but now with the same color coding of these different branches as in Figure 5.5. Note that for nonzero detuning there are no constant-phase CLMs. Nevertheless, we see that there are two substantial sections of the branch where the CLM has almost constant phase of $\sigma \approx 0$ and $\sigma \approx \pi$. These parts are connected by sections where the phase increases and decreases, respectively. These different sections can be identified as the reminders of corresponding constant-phase and intermediate-phase CLMs for zero detuning, which is clearly brought out by the coloring. Considering the right column and decreasing C_p, a pair of CLMs is born in the saddle-node bifurcation at $C_p \approx 2.7\pi$. The purple branch has almost constant phase $\sigma \approx \pi$ while the dark green branch has a decreasing phase σ. A second pair of CLMs is born in the saddle node at $C_p \approx 1.8\pi$. The pink branch has almost constant phase $\sigma \approx 0$, while the light green branch has an increasing phase σ. The decreasing-phase and the increasing-phase branches cross and the branches come together differently in the other two saddle-node bifurcations on the left. This scenario corresponds to moving over the respective branches of the same color in the left column of Figure 6.4.

Clearly, Figure 6.4(a1)–(c1) and Figure 6.4(a2)–(c2) are a perturbation, resulting in unfoldings the pitchfork bifurcations, of the respective plots for zero detuning in the Figure 5.4(a) and (b). To show in detail which branches interact in this unfolding of the pitchfork bifurcations Figure 6.5 shows enlarged views in the (C_p, N^s)-plane. The left column shows the situation for zero detuning, where the constant-phase CLMs (pink and purple curves) have $N_1^s = N_2^s$. The inversions of the intermediate-phase CLMs (dark green and light green curves) lie on the same curve but at different positions because $N_1^s \neq N_2^s$. Consequently, as was discussed earlier, every branch that exists for nonzero detuning 'doubles' in the presence of detuning, as can be seen in the right column of Figure 6.5. The different rows show clearly how different branches connect locally near the pitchfork bifurcations, which globally leads to the structure of CLMs in Figure 6.4.

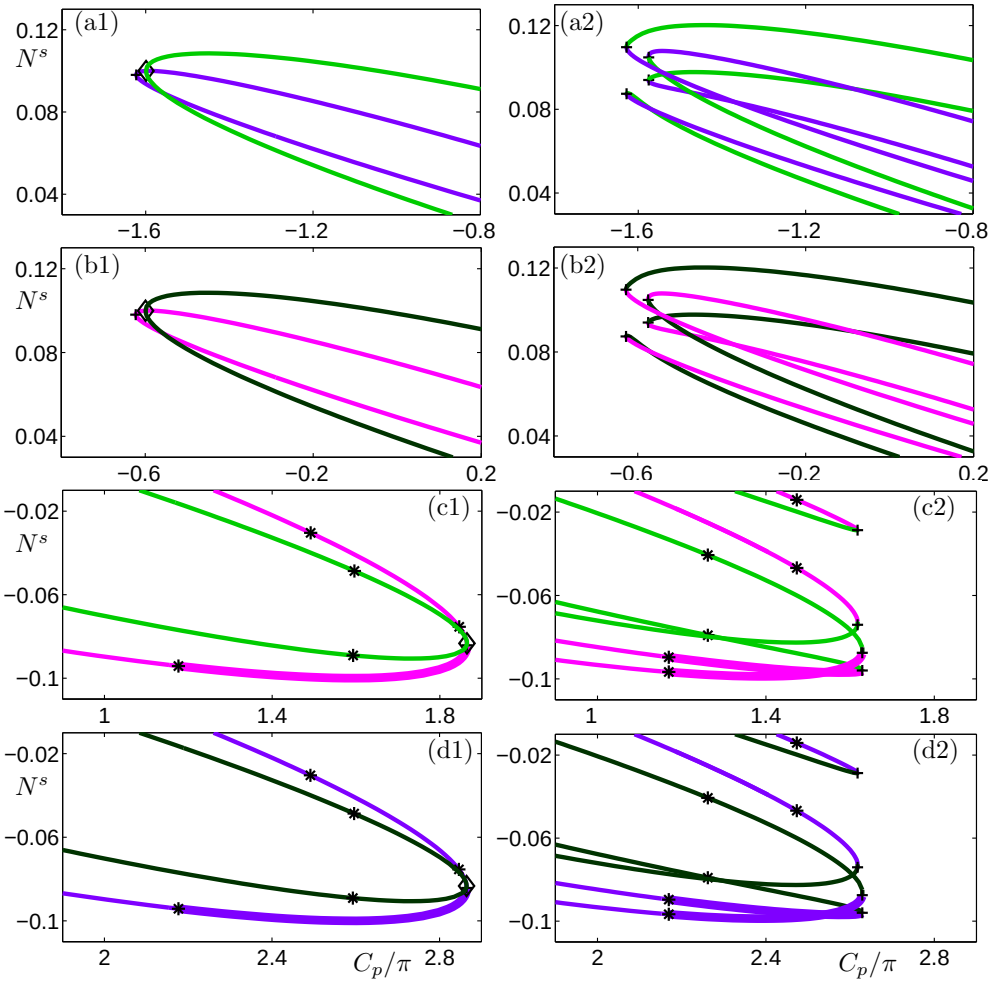

FIG. 6.5. *Enlarged views of branches of CLMs for* $\Delta = 0.025$ *in the* (C_p, N^s)*-plane near the unfoldings of pitchfork bifurcations showing how different types of branches connect.*

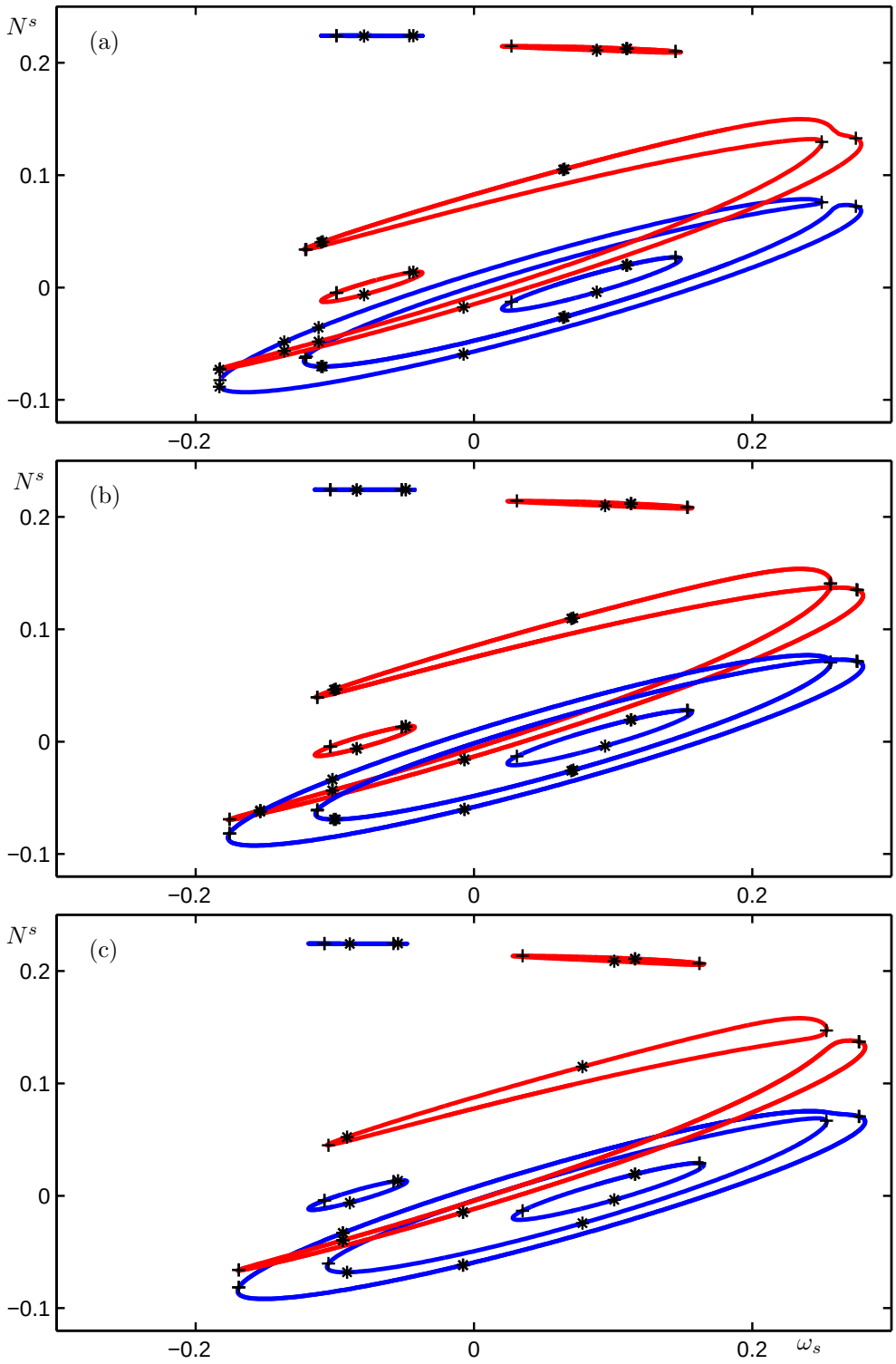

FIG. 6.6. *Detuning sequence of CLMs in the (ω^s, N^s)-plane showing the inversions of the red and blue lasers during a transition through a saddle singularity. From (a) to (c) Δ takes the values 0.075, 0.080 and 0.085. See also the accompanying animations ekl_a3.gif and ekl_a4.gif.*

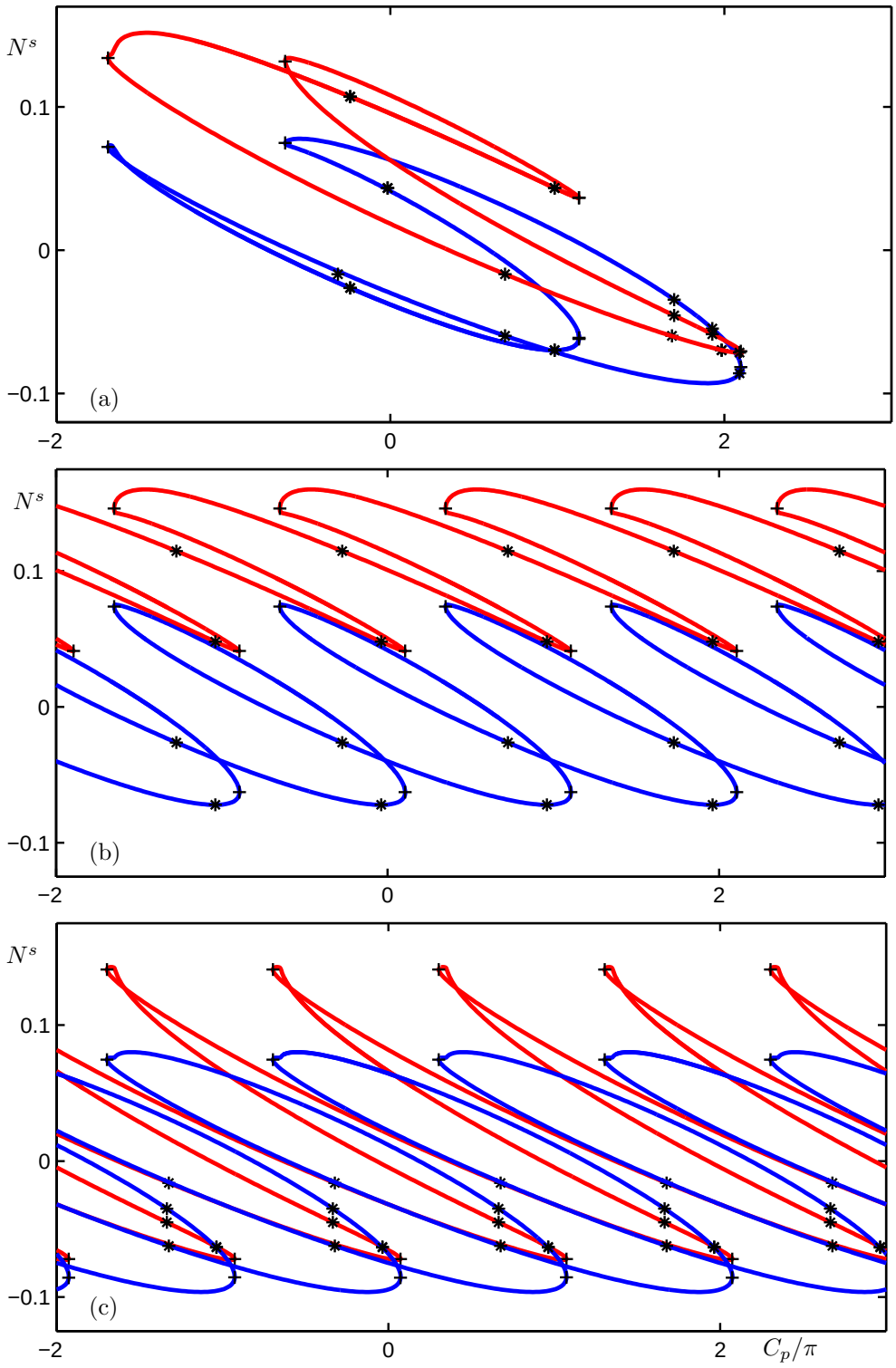

FIG. 6.7. *Panel (a) shows the curves of CLMs from Figure 6.6 in the* (C_p, N^s)*-plane before the transition for* $\Delta = 0.075$*, while panels (b) and (c) show two types of curves of CLMs for* $\Delta = 0.085$ *that created in the saddle transition.*

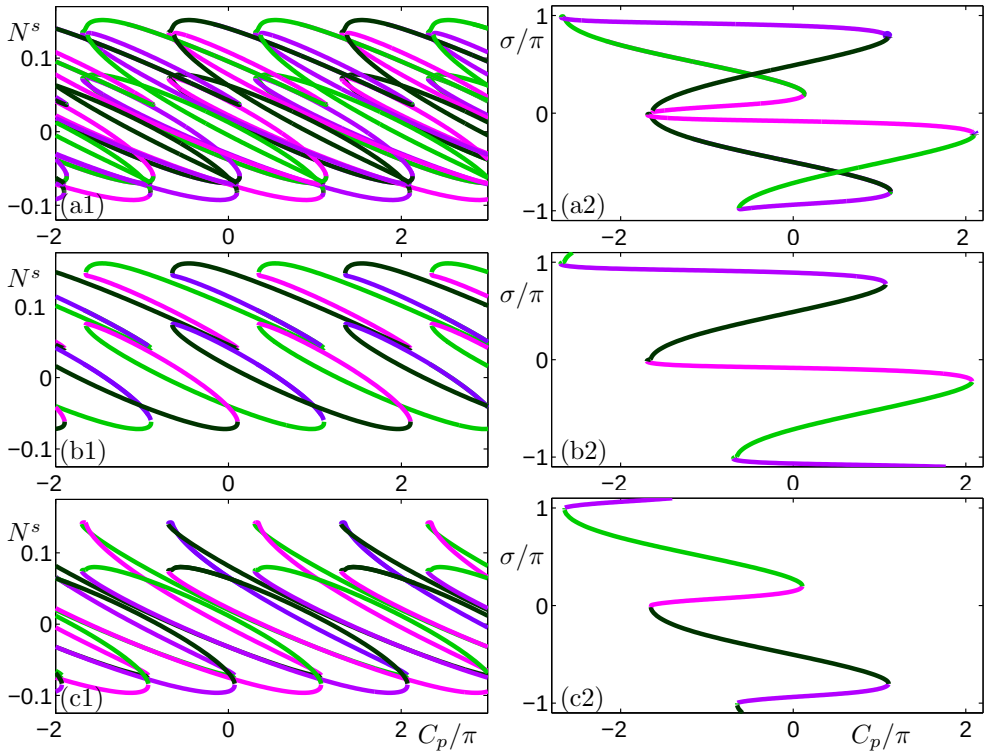

FIG. 6.8. *The curves of CLMs from Figure 6.7 in the (C_p, N^s)-plane (left column) and in the (C_p, σ)-plane (right column), where the different branches are color coded as in Figure 5.4 to identify (approximate) in-phase, anti-phase, increasing-phase, and decreasing-phase CLMs.*

6.2. Intermediate Values of Detuning. As we see now, branches of CLMs connect or disconnect for larger values of the detuning Δ. In Figure 6.6 all branches of CLMs are shown in the (ω^s, N^s)-plane, for three different intermediate values of Δ. This figure reveals a 'pinching-off' of the red horseshoe, while the blue horseshoe transforms into two concentric circles. Figure 6.6(b) shows a transversal crossing of the respective parts of the red and blue curves.

The transition can be understood in terms of the corresponding red and blue surfaces in (C_p, Δ, N^s)-space. In fact, Figure 6.6(b) already shows that we are dealing with a crossing through a saddle singularity of this surface with respect to Δ. This is a classic codimension-one singularity of this surface [8] that leads locally to a different reconnection of the branches involved. In Figure 6.7 we show how this manifests itself in the (C_p, N^s)-plane in terms of the inversions of the red and blue lasers. Panel (a) shows the situation for $\Delta = 0.075$, which corresponds to Figure 6.3(a). As the saddle-singularity is approached, two π-translational symmetry related CLM branches approach each other. After the singularity there are two separate branches of CLMs, that is, pairs of red and blue branches. They are plotted in Figure 6.7(b) and (c), respectively.

In Figure 6.8 we plot the curves of CLMs of Figure 6.7 in the (C_p, N^s)-plane (left column) and the (C_p, σ)-plane (right column), again with the same color coding indicating the different branches in terms of their phase difference σ. Furthermore, we

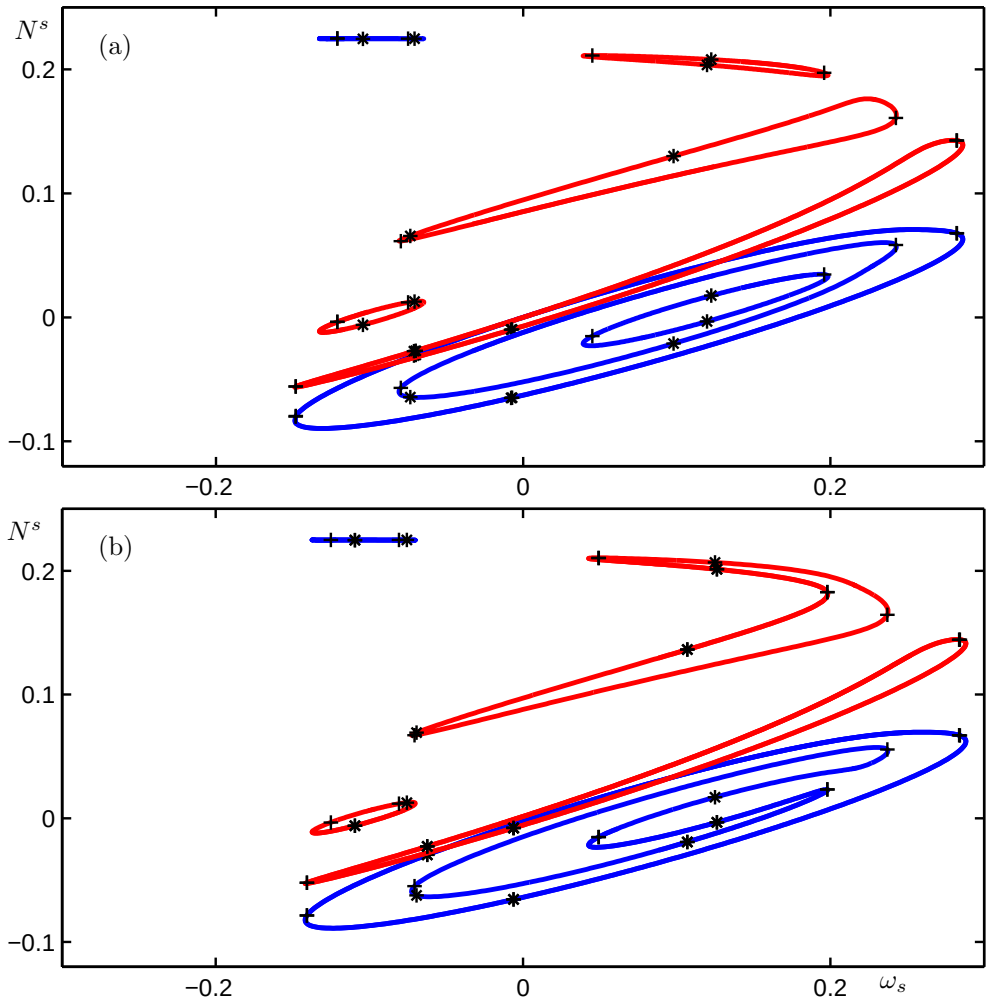

FIG. 6.9. *Detuning sequence of CLMs in the (ω^s, N^s)-plane for the red and blue lasers before (a) and after (b) a further transition through a saddle singularity; the detuning Δ takes the values 0.10 and 0.105, respectively. See also the accompanying animations ekl_a3.gif and ekl_a4.gif.*

now plot in panel (a) all copies of branches under the translational symmetries. As the saddle-singularity is approached, two π-translational symmetry related CLM branches approach each other; see the region around $(C_p, \sigma) = (-1.8, 0)$ in Figure 6.8(a1). After the transition we see that the first CLM branch in Figure 6.8(b) is formed by connecting the upper dark green branch with the lower pink branch, while the second CLM branch in Figure 6.8(b) is formed by connecting the lower dark green branch with the upper pink branch. Note that both branches do not have a bounded phase difference as a function of C_p.

The physical interpretation of this transition through a saddle singularity is as follows. Detuning has the tendency to pull the inversions of the two lasers apart, whereas the coupling ties them together. Before the saddle-singularity the system can unify both tendencies in a single branch of CLMs; see Figures 6.7(a) and 6.8(a). However, after the saddle-singularity there are two different branches of CLMs. The

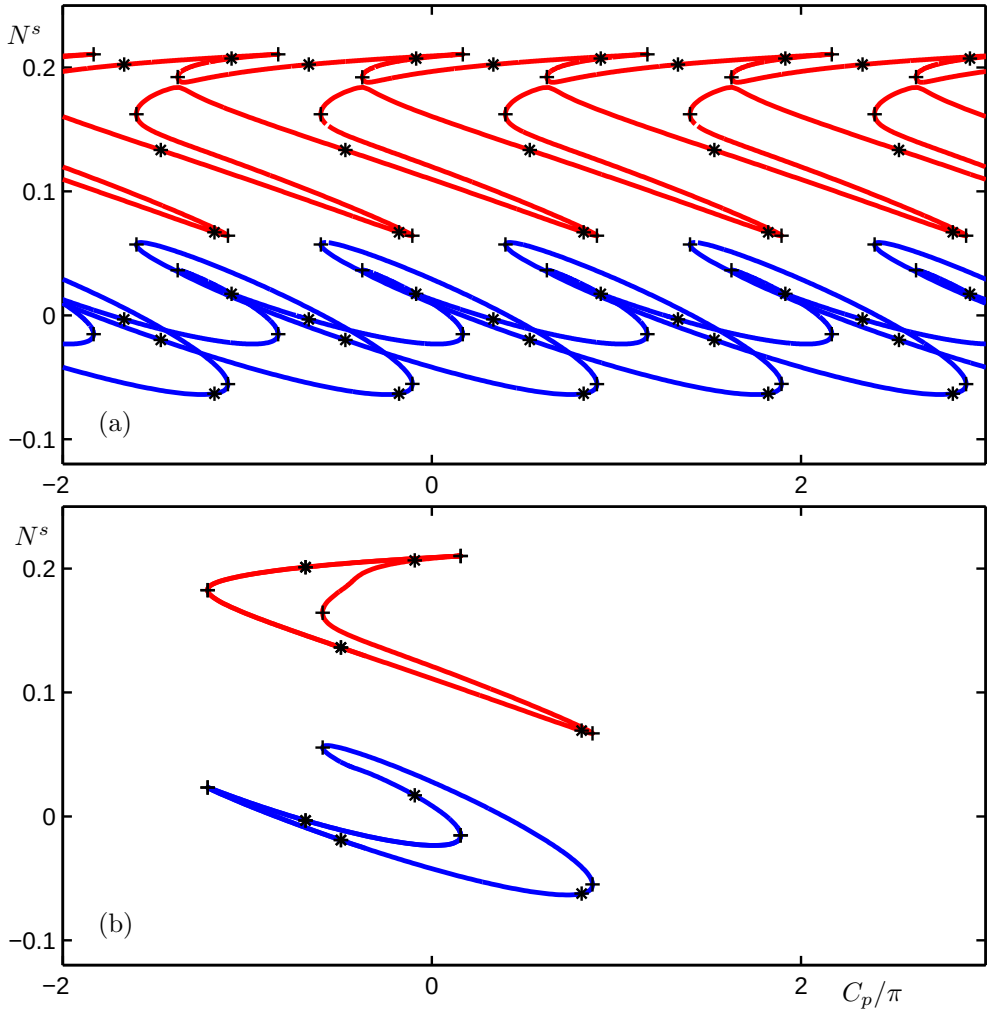

FIG. 6.10. *The curves of CLMs from Figure 6.9 in the (C_p, N^s)-plane (left column) and in the (C_p, σ)-plane (right column), where the different branches are color coded as in Figure 5.4 to identify (approximate) in-phase, anti-phase, increasing-phase, and decreasing-phase CLMs.*

branch in Figures 6.7(b) and 6.8(b) corresponds to the 'pulling-apart-tendency' of the detuning, while the one in Figures 6.7(c) and 6.8(c) corresponds to the 'tying-together-tendency' of the coupling. Note that at the saddle singularity we are dealing with two CLMs with the same inversion, which is also known as the Petermann-Tager condition in the context of a laser with conventional optical feedback [34, 38].

When Δ is increased even further we encounter a second saddle-singularity. However, this time the global organization of the branches of CLMs is such that this results in the merging of two separate branches. In Figure 6.9 all branches of CLMs are shown in the (ω^s, N^s)-plane, for two different values of detuning, one before and one after this second saddle-singularity. While the exact shape and position of the different branches of CLMs has changed, the situation in Figure 6.9(a) is topologically as that in Figure 6.6(c). After the bifurcation the two separate red branches merged

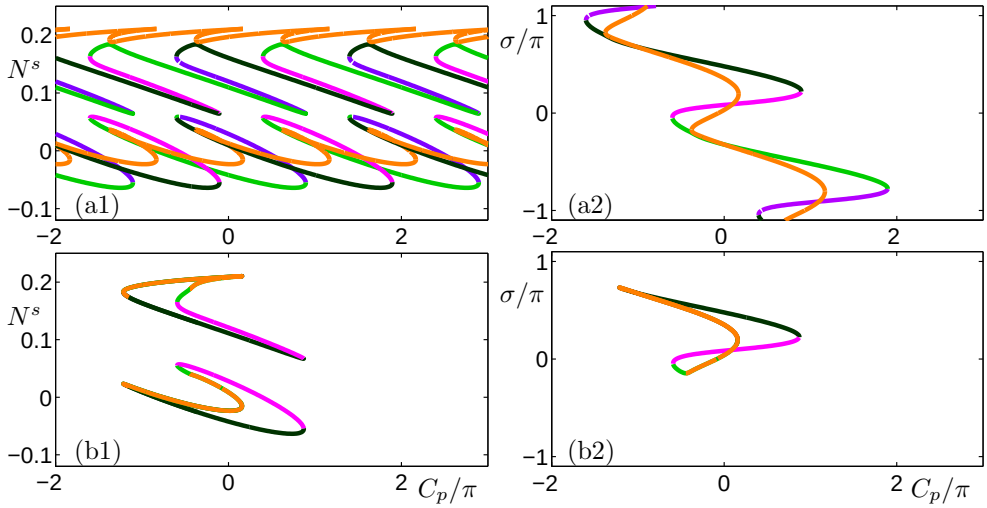

FIG. 6.11. *The curves of CLMs from Figure 6.9 in the* (C_p, N^s)*-plane.*

into a 'boomerang-like' structure, while the two innermost concentric blue curves form a new horseshoe.

In the (C_p, N^s)-plane this transition manifests itself as shown in Figure 6.10 in terms of the inversions of the red and blue lasers. Figure 6.11 again shows the branches of CLMs in the (C_p, N^s)-plane and the (C_p, σ)-plane in the color coding in terms of the phase difference σ. Before the saddle-singularity there are exactly two distinct branches of CLMs, that is pairs of red and blue curves in Figure 6.10. As the singularity is approached the low-inversion branch of the red laser hits the high-inversion branch from below. Then these two branches connect differently to form infinitely many closed red curves, and the two blue curves undergo a similar transition to infinitely many bounded, closed curves; see Figure 6.10(b) and also Figure 6.11(b1). In the process, the phase difference between the two lasers becomes bounded, as is shown in Figure 6.11(b2).

6.3. The Limit of Very Large Detuning. When Δ is increased even further, as is shown in Figure 6.12 in the (ω^s, N^s)-plane, then a pair of red and blue islands, that is, a separate branch of CLMs, shrink down to a two points and disappear. This happens in another classical codimension-one singularity of the surface of CLMs, namely a transition through an extremum [8]. Specifically, a maximum with respect to Δ. After this last singularity transition the situation remains topologically the same. However, the remaining two pairs of isolas become smaller and smaller and they center around the points $(\omega^s, N^s) \approx (\pm\Delta, 0)$ and $(\omega^s, N^s) \approx (\pm\Delta, P)$.

This behavior can be explained by considering the limit of Δ going to infinity. Clearly, $R^s_{1,2}$, $N^s_{1,2}$, ω^s and σ^s in Equations (3.5)–(3.10) depend on Δ; we denote their limiting values for $\Delta \to \infty$ by $\overline{R}^s_{1,2}$, $\overline{N}^s_{1,2}$, $\overline{\omega}^s$ and $\overline{\sigma}^s$, respectively. By solving Equation (3.11) for $1/\Delta^2$ we conclude that $(\omega^s)^2$ grows as Δ^2. In other words, in the limit $\Delta \to \infty$ we have that

$$\overline{\omega}^s = \pm\Delta\,. \tag{6.1}$$

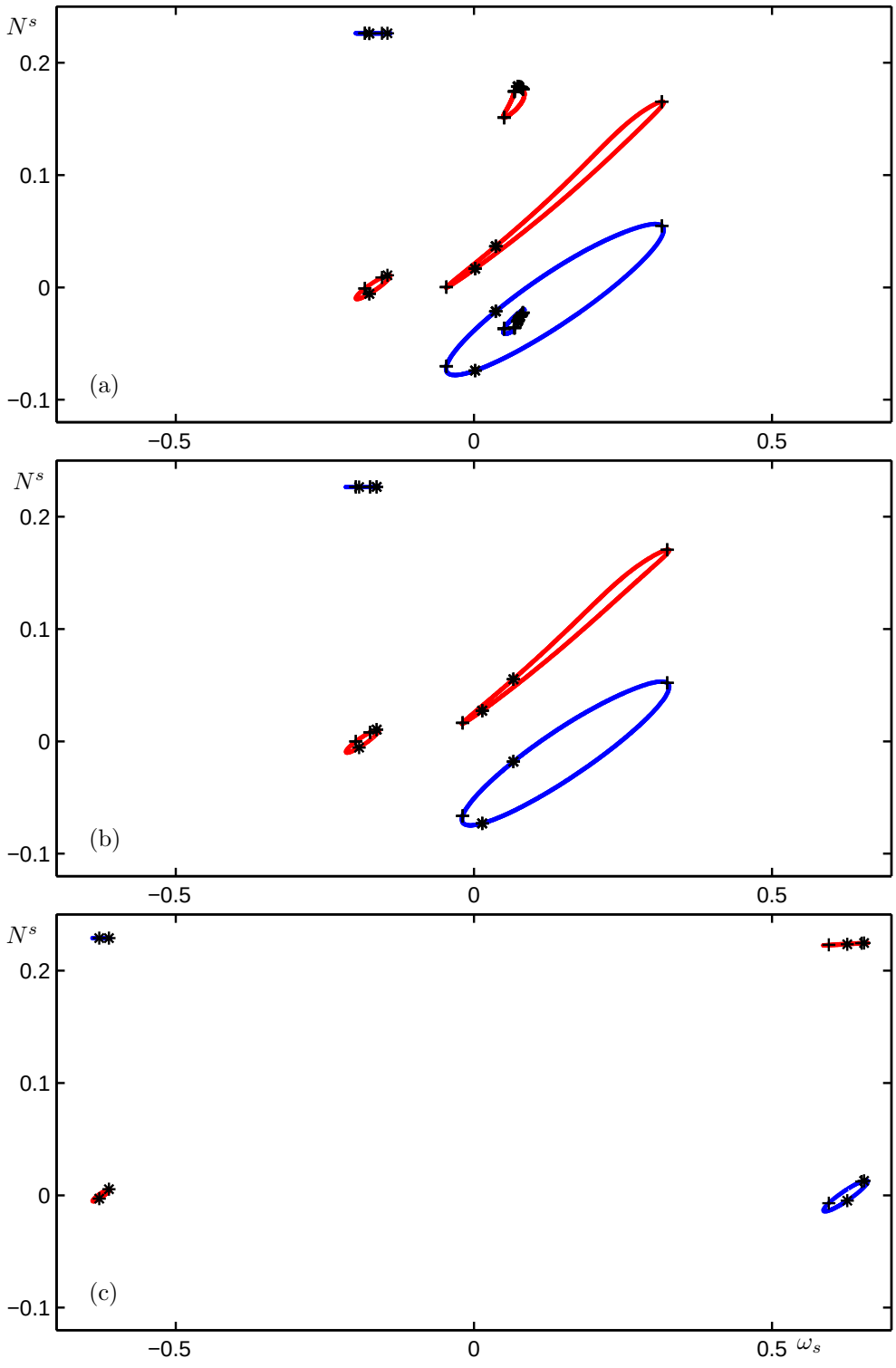

FIG. 6.12. *Detuning sequence of CLMs in the* (ω^s, N^s)*-plane for the red and blue lasers towards the limit of large detuning; from (a) to (c)* Δ *takes the values 0.17, 0.1875 and 0.625. Notice the transition through a maximum between panels (a) and(b) in which a pair of closed branches disappears. See also the accompanying animations ekl_a3.gif and ekl_a4.gif.*

Due to the symmetry (2.6) it is sufficient to consider only the case $\Delta = \omega^s$. We use (3.5) and (3.6) for $\overline{\omega}^s = \Delta$ to eliminate N_1^s and obtain

$$2\Delta = \kappa\sqrt{(1+\alpha^2)}\frac{R_2^s}{R_1^s}\sin(-C_p - \Delta\tau + \sigma - A_\alpha)\,, \tag{6.2}$$

where $A_\alpha = \arctan\alpha$. Taking reciprocals and letting $\Delta \to \infty$, we conclude that

$$\frac{\overline{R}_1^s}{\overline{R}_2^s} = 0\,. \tag{6.3}$$

Inserting this limit into Equation (3.7) gives, for $\overline{\omega}^s = \Delta$,

$$\overline{N}_2^s = 0\,. \tag{6.4}$$

Finally, combining Equations (3.9) and (3.10) gives

$$\frac{|R_1^s|^2}{|R_2^s|^2} = \frac{(1+2N_2^s)(P-N_1^s)}{(1+2N_1^s)(P-N_2^s)}\,, \tag{6.5}$$

from which we conclude with Equations (6.3) and (6.4) that

$$\overline{N}_1^s = P\,. \tag{6.6}$$

The amplitudes R_1^s and R_2^s are computed from Equations (3.9) and (3.10) as

$$\overline{R}_1^s = 0 \quad \text{and} \quad \overline{R}_2^s = P \tag{6.7}$$

Recall that R_1^s and R_2^s are defined to be positive.

This result on the limit $\Delta \to \infty$ can be interpreted physically as follows. Because of the mismatch in their free-running optical frequencies, the electric field of one laser has a decreasing influence on the electric field of the other laser. When Δ grows, the two lasers are more and more detuned. Concentrating on the solution on the positive side of the ω^s-axes in Figure 6.12 it can be seen that the red detuned laser operates around its detuned free running optical frequency. Due to the coupling the blue laser is forced to also operate at this frequency, that is it is far away from its detuned free running optical frequency. Therefore, the blue laser operates around its off state. In turn this means that the effective coupling between the lasers is small and the red laser is only perturbed little. In the limit $\Delta \to \infty$ the two lasers are completely independent. This is expressed in Equations (2.1)–(2.4) as two solutions: the red laser is on and the blue laser is off, or vice versa.

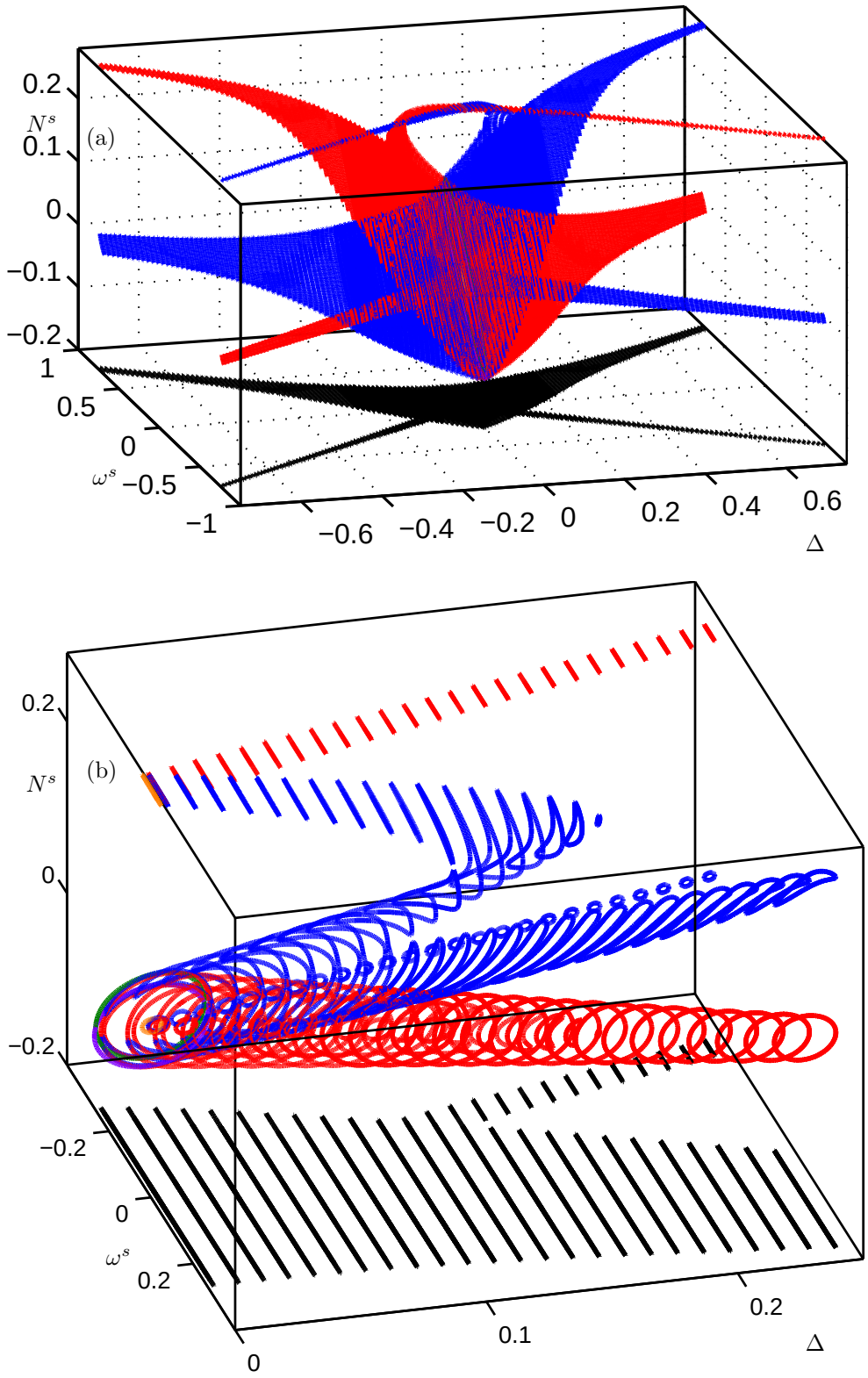

FIG. 6.13. *The surface of CLMs in* (Δ, ω^s, N^s)*-space for* $\Delta \in [-0.6, 0.6]$ *as built up from 150 equidistant* Δ*-slices (a), and an enlarged view for positive* Δ*(b). The inversion of laser 1 is shown in red and that of laser 2 in blue; the projection of the CLMs onto the* (Δ, ω^s)*-plane is shown in black.*

6.4. The surface of CLMs. To get an overall impression of of the CLM structure we give in Figure 6.13 an impression of the corresponding surfaces in (Δ, ω^s, N^s)-space. As before, the inversion of laser 1 is plotted in red and that of laser 2 in blue; the projection of the surface of CLMs onto the (Δ, ω^s)-plane is shown in black. The image is built up from 150 Δ-slices that were computed with DDE-BIFTOOL which also form the frames of the accompanying animation ekl_a4.gif. Panel (a) shows the whole structure for $\Delta \in [-0.6, 0.6]$. The blue surface is mapped to the red surface and vice versa by the symmetry (2.6) of exchanging the two lasers and changing the sign of Δ. The two surfaces intersect for $\Delta = 0$. For small Δ this surface has a complicated, nested structure. This can be seen in panel (b), where an enlarged view for positive Δ is shown. For increasing (or decreasing) detuning the nested structure starts to disentangle. Indeed this process proceeds as described in Section 6.2 with transitions through saddle singularities. A saddle can be seen clearly on the blue surface in Figure 6.13(b). Furthermore, one clearly notices the extremum, specifically a maximum with respect to Δ, on the same blue surface where the surface 'bends back' to decreasing Δ. The limiting behavior of the CLMs, as discussed in Section 6.3, is brought out well by Figure 6.13(a).

The black projection onto the (Δ, ω^s)-plane shows the parameter region where CLMs exist. As was explained in the previous section, ω^s is not a bifurcation parameter, so that the boundaries of the projection are not saddle-node bifurcations. Nevertheless, the saddle-node bifurcations are close to the folds with respect to ω^s. Figure 6.14 shows the curves of saddle-node bifurcations (blue) and the curve of the first Hopf bifurcation (red) that forms a boundary of the region of stable CLMs for small detuning. Panel (a) shows the (Δ, ω^s)-plane for $\Delta \in [-0.7, 0.7]$ and panel (b) is an enlarged view around the stable region (green).

Figure 6.15 shows the same bifurcation curves in the (Δ, C_p)-plane. In panel (a) we only plot the basic structure once, while in panel (b) we also show all its images under the π-translational symmetry of the system. There is a complicated structure of different regions, especially near the stable region, as can be seen in the further enlargement in panel (c). Overall, there are two closed curves of saddle-node bifurcations. The first branch of saddle-node bifurcations is limited to a detuning interval of $\Delta \approx [-0.23, 0.23]$; it arises in the unfolding of the pitchfork bifurcation of intermediate-phase CLMs (green curves in Section 5). Indeed this shows that the saddle-node bifurcations of the constant-phase CLMs (purple curves in Section 5) are connected with the second set of intermediate-phase CLMs (orange curves in Section 5). The second branch of saddle-node bifurcations traces out the large 'triangular' curve. There are a number of cusp bifurcations on the saddle-node curves, so that different branches correspond to saddle-node bifurcations of different CLMs. Note that the cusp points do not appear as cusps in the projection onto the (Δ, ω^s)-plane in Figure 6.14.

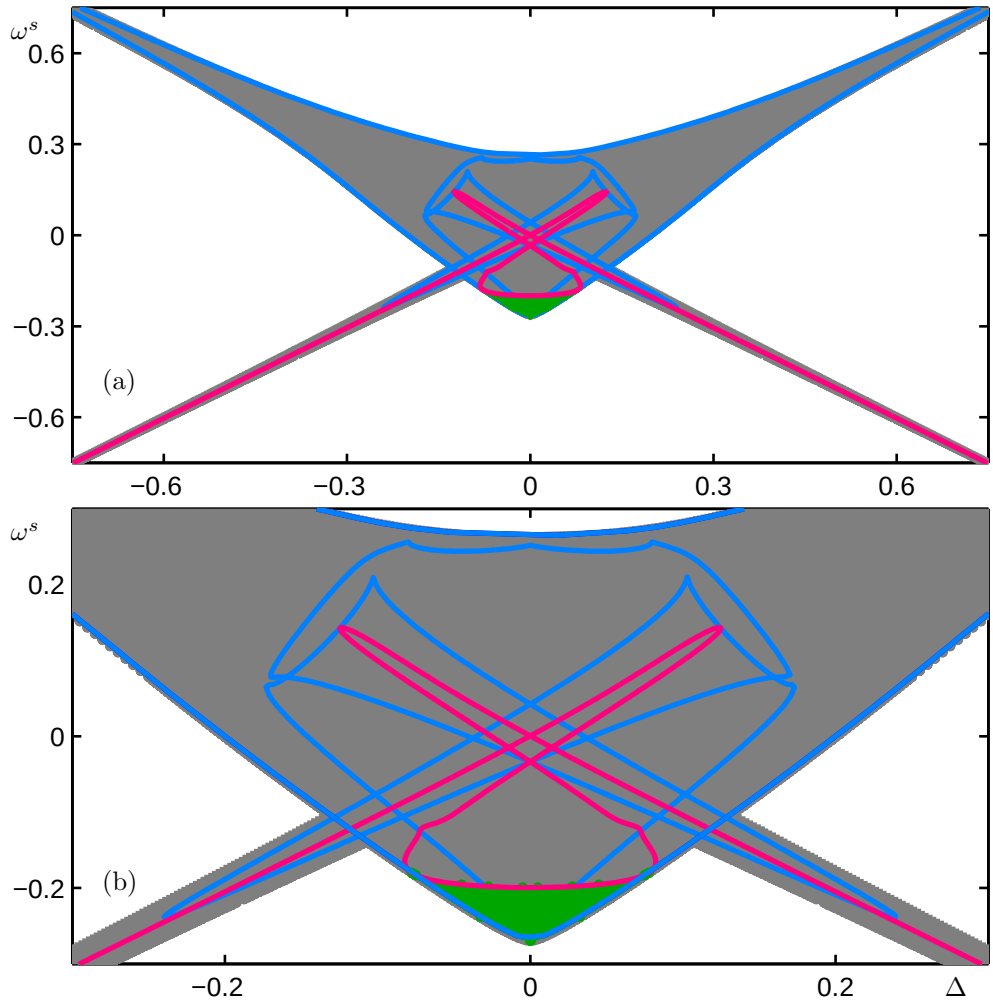

FIG. 6.14. *Two-parameter bifurcation diagram in the* (Δ, ω^s)*-plane with saddle-node bifurcation curves (blue) and the curve of the first Hopf bifurcation (red). The region where CLMs exist is shaded in gray and the region of stable CLMs is plotted in green. Panel (b) shows enlarged view of panel (a).*

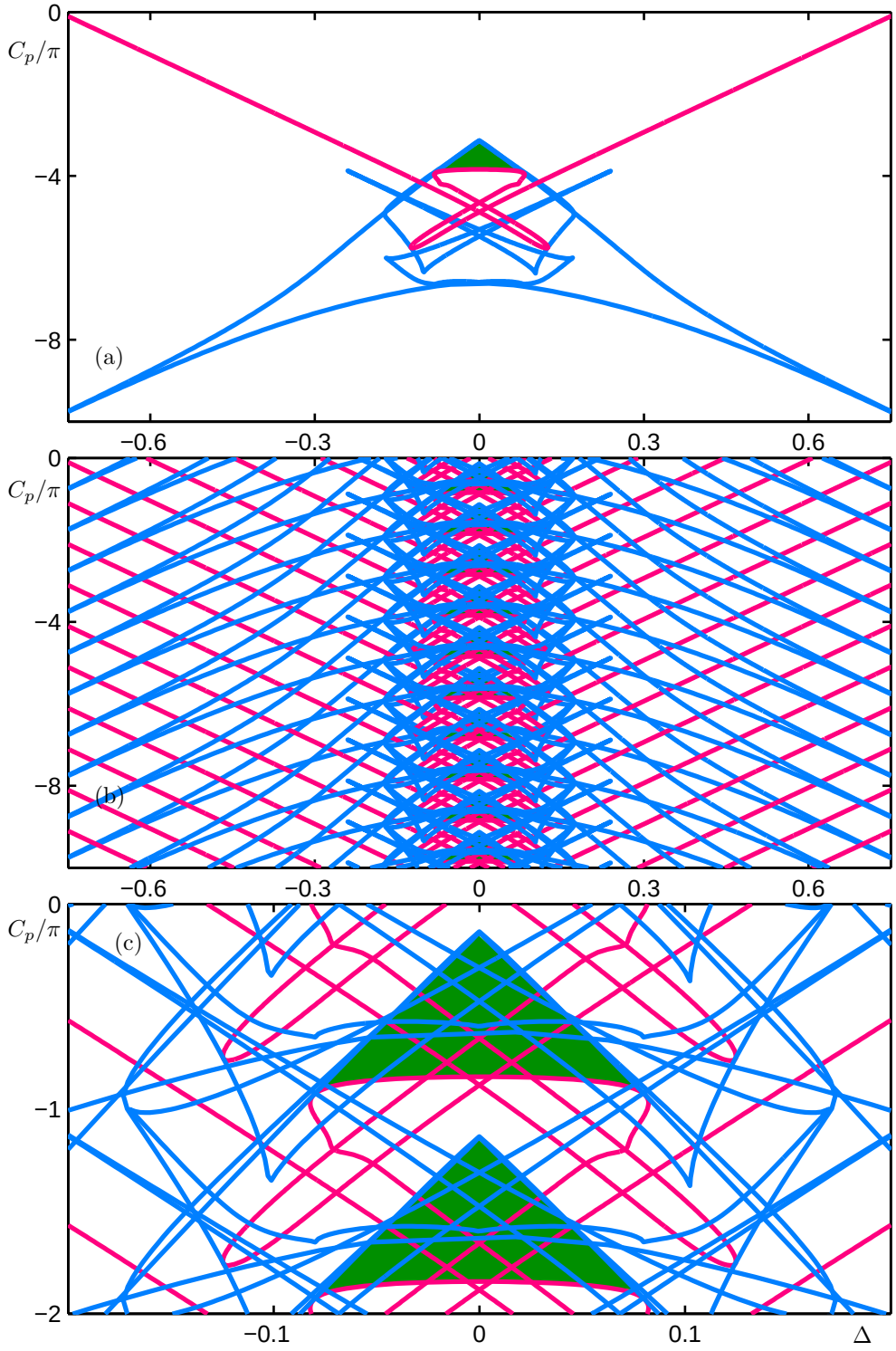

FIG. 6.15. *Two parameter bifurcation diagram in the (Δ, C_p)-plane with saddle-node bifurcation in blue and Hopf bifurcation in red. The region of stable CLMs in plotted in green. Panel (a) shows the the basic structure, Panel (b) take the translational symmetries into account, and panel (c) show an enlarged view of panel (b).*

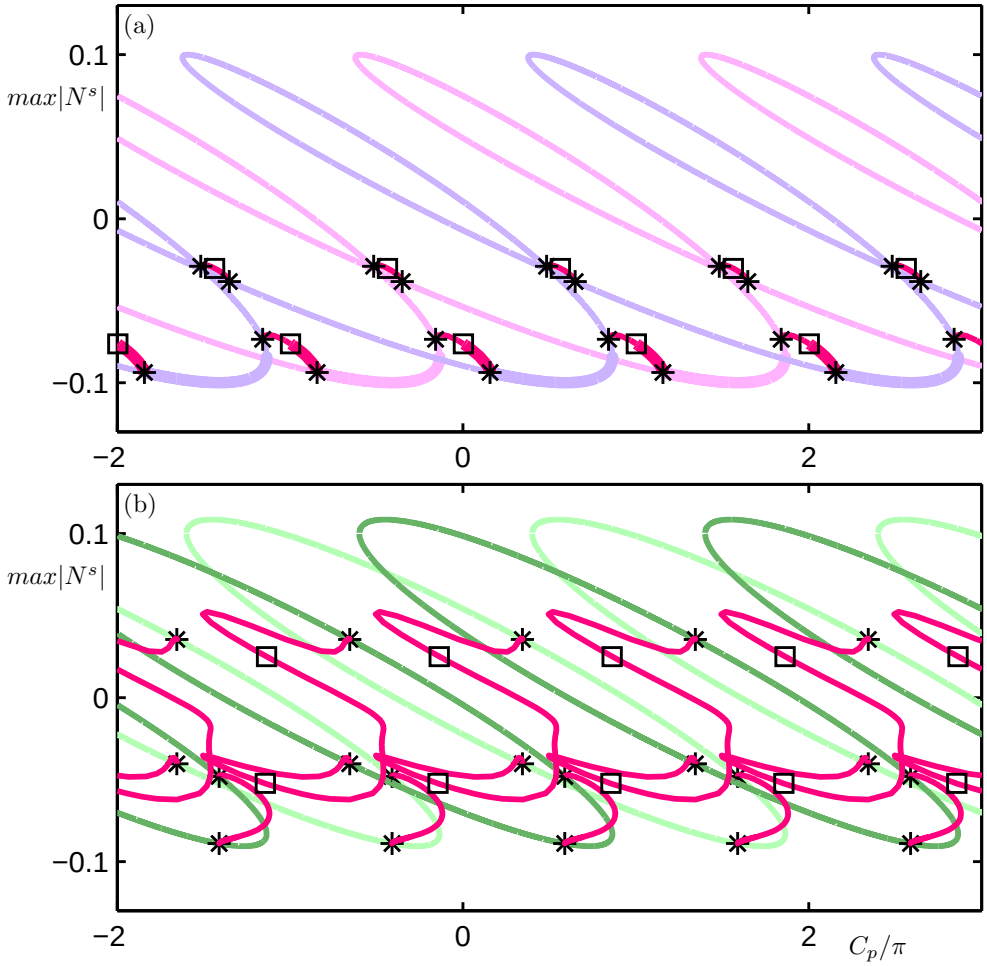

FIG. 6.16. *Branches of periodic solutions (red) in the (C_p, N^s)-plane. Plotted is the amplitude of the periodic solution; stable parts are boldfaced. Periodic solutions emerge from Hopf bifurcations ($*$) of CLMs and destabilize in torus bifurcations ($\square$). The branches of in-phase, anti-phase, increasing-phase, and decreasing-phase CLMs are shown in lighter colors; compare Figure 5.4.*

7. Outlook. We presented here a comprehensive geometric picture of the CLMs of two identical delay-coupled lasers in dependence of the feedback phase and the detuning. This revealed a complicated structure of different types of CLMs, which form the 'backbone' of all dynamics in the system. Clearly, there are a number of interesting topics for further studies.

First of all, it is now possible to consider the periodic orbits that are born in Hopf bifurcations. Near the stable region of constant-phase CLMs one finds stable oscillations of the power that can then bifurcate further. To give an idea, we present in Figure 6.16 branches of periodic orbits in the (C_p, N^s)-plane that bifurcate from branches of constant-phase CLMs, in panel (a), and from branches of intermediate-phase CLMs, in panel (b). The branches of constant-phase and intermediate-phase CLMs are repeated from Figure 5.4 and plotted in a lighter color. The constant-phase CLMs exhibit four different Hopf bifurcation points in total; the symmetric copies are

not taken into account. These Hopf bifurcations are connected in pairs by branches or 'bridges' of periodic orbits. Branches of periodic orbits (red curves) are represented by plotting the maximum amplitude of the oscillation; stable parts are boldfaced. A similar picture emerges for the intermediate-phase CLMs plotted in Figure 6.16(b). They also exhibit four different Hopf bifurcations, which are pairwise connected by branches of periodic orbits.

The situation for the constant-phase CLMs is similar to the case of the Lang-Kobayashi equations for a laser with conventional optical feedback where one finds 'bridges' of periodic orbits that connect different branches of external cavity modes [10]. However, in the present situation it emerges that such bridges of periodic orbits provide a connection between different types of CLMs. Concentrating on the smaller branch of periodic orbits emerging from the Hopf bifurcation of the constant-phase CLMs, it can be seen that this branch connects two Hopf bifurcations that are located near the intersection of an in-phase CLM branch and an anti-phase CLM branch, respectively. This branch of periodic orbits is unstable throughout, but there is a torus bifurcation point on it. The longer branch of periodic orbits connects two Hopf bifurcations near the intersection of an in-phase CLM with an anti-phase CLMs; one Hopf bifurcation is on the branch of the in-phase CLMs and the other one is on the branch of the anti-phase CLMs. This branch of periodic orbits is initially stable, so that one observes stable oscillations of the power of the two lasers. As C_p is decreased it destabilizes in a torus bifurcation, giving rise to stable quasiperiodic or locked oscillations of the laser power. This torus then breaks up and gives rise to a region of chaotic fluctuations. A more detailed study of connecting bridges and associated routes to chaos is an interesting topic of ongoing research.

Another important question is how similar the two lasers need to be. Indeed, it is practically impossible to produce two identical lasers. On the other hand, present experiments [5, 6, 37] show good agreement with the model as studied here. In other words, apparently it is sufficient that the lasers are similar enough in terms of their material properties. By performing a bifurcation study in the parameters α and T it is possible to study this question systematically.

Acknowledgments. The research of B.K. was supported by an Engineering and Physical Sciences Research Council (EPSRC) Advanced Research Fellowship grant.

REFERENCES

[1] G. A. Agrawal and N. K. Dutta, *Long-Wavelength Semiconductor Lasers*, Van Nostrand Reinhold, 1986.

[2] O. Diekmann, S. A. V. Gils, and S. M. V. Lunel, *Delay Equations: Functional-, Complex-, and Nonlinear Analysis*, Springer Verlag, New York, 1995.

[3] E. J. Doedel, R. Paffenroth, A. R. Champneys, T. F. Fairgrieve, Y. A. Kuznetsov, B. E. Oldeman, B. Sandstede, and X. Wang, *AUTO 2000: Continuation and Bifurcation Software for Ordinary Differential Equations (with HomCon)*, http://sourceforge.net/projects/auto2000/, 2000.

[4] K. Engelborghs, T. Luzyanina, and G. Samaey, *DDE-BIFTOOL v. 2.00 user manual: a matlab package for bifurcation analysis of delay differential equations.*, Technical Report TW-330, Department of Computer Science, K. U. Leuven, Leuven, Oct. 2001.

[5] H. Erzgräber, D. Lenstra, B. Krauskopf, and I. Fischer, *Dynamical properties of mutually delayed coupled semiconductor lasers in: 'semiconductor lasers and laser dynamics*, Proceedings of SPIE, 5452 (2004), pp. 352–361.

[6] H. Erzgräber, D. Lenstra, B. Krauskopf, E. Wille, M. Peil, I. Fischer, and Elsässer, *Mutually delay-coupled semiconductor lasers with short coupling times: bifurcation scenarios in the locking regime*, submitted (2004).

[7] I. Fischer, Y. Liu, and P. Davis, *Synchronization of chaotic semiconductor laser dynamics on subnanosecond time scales and its potential for chaos communication*, Phys. Rev. A, 62 (2000), p. 011801.
[8] M. Golubitsky and D. G. Schaeffer, *Singularities and groups in bifurcation theory I*, Springer Verlag, Heidelberg, 1998.
[9] K. Green, B. Krauskopf, and G. Samaey, *A two-parameter study of the locking region of a semiconductor laser subject to phase-conjugate feedback*, SIAM Journal of Applied Dynamical Systems, 2(2) (1992), pp. 254–276.
[10] B. Haegeman, K. Engelborghs, D. Rose, D. Pieroux, and T. Erneux, *Stability and rupture of bifurcation bridges in semiconductor lasers subject to optical feedback*, Phys. Rev E, 66 (2002), p. 046216.
[11] J. K. Hale and S. M. V. Lunel, *Introduction to Functional Differential Equations*, Springer Verlag, New York, 1993.
[12] T. Heil, I. Fischer, W. Elsässer, and A. Gavrielides, *Dynamics of semiconductor lasers subject to delayed optical feedback: The short cavity regime*, Phys. Rev. Lett., 87 (2001), p. 243901.
[13] T. Heil, I. Fischer, W. Elsässer, J. Mulet, and C. R. Mirasso, *Chaos synchronization and spontaneous symmetry-breaking in symmetrically delay-coupled semiconductor lasers*, Phys. Rev. Lett., 86 (2001), pp. 795–798.
[14] A. Hohl, A. Gavrielides, T. Erneux, and V. Kovanis, *Localized synchronization in two coupled nonidentical semiconductor lasers*, Phys. Rev. Lett., 78 (1997), pp. 4745–4748.
[15] ———, *Quasiperiodic synchronization for two delay-coupled semiconductor lasers*, Phys. Rev. A, 59 (1999), pp. 3941–3949.
[16] J. Javaloyes, P. Mandel, and D. Pieroux, *Dynamical properties of lasers coupled face to face*, Phys. Rev. E, 67 (2003), p. 036201.
[17] B. Krauskopf, *Bifurcation analysis of lasers with delay*, Unlocking Dynamical Diversity: Optical Feedback Effects on Semiconductor Lasers (D. M. Kane and K. A. Shore; Eds), Wiley, to appear (http://www.enm.bris.ac.uk/anm/preprints/2003r12.html).
[18] B. Krauskopf, H. Erzgräber, and D. Lenstra, *Bifurcation analysis of coupled laser modes in mutually delay-coupled lasers*, 5th IFAC Workshop on Time-Delay Systems, 2004.
[19] B. Krauskopf and D. Lenstra, *Fundamental Issues of Nonlinear Lasers Dynamics*, American Institute of Physics, 2000.
[20] B. Krauskopf, G. H. M. V. Tartwijk, and G. R. Gray, *Symmetry properties of lasers subject to optical feedback*, Opt. Commun., 177 (2000), pp. 347–353.
[21] R. Lang and K. Kobayashi, *External optical feedback effects on semiconductor injection laser properties*, IEEE J. Quantum Electron., QE-16 (1980), pp. 347–355.
[22] J. Mulet, C. Masoller, and C. R. Mirasso, *Modeling bidirectionally coupled single-mode semiconductor lasers*, Phys. Rev. A, 65 (2002), p. 063815.
[23] J. Mulet, C. Mirasso, T. Heil, and I. Fischer, *Synchronization scenario of two distant mutually coupled semiconductor lasers*, J. Opt. B: Quantum Semiclass. Opt., 6 (2004), pp. 97–105.
[24] D. Pieroux and P. Mandel, *Bifurcation diagram of a complex delay-differential equation with cubic nonlinearity*, Phys. Rev. E, 67 (2003), p. 056223.
[25] A. Pikovsky, M. Rosenblum, and J. Kurths, *Synchronization: a Universal Concept in Nonlinear Sciences*, Cambridge University Press, 2001.
[26] D. V. Ramana Reddy, A. Sen, and G. L. Johnston, *Time delay induced death in coupled limit cycle oscillators*, Phys. Rev. Lett., 80 (1998), pp. 5109–5112.
[27] F. Rogister and J. Garca-Ojalvo, *Symmetry breaking and high-frequency periodic oscillations in mutually coupled laser diodes*, Opt. Lett., 28 (2003), pp. 1176–1178.
[28] V. Rotschäfer and B. Krauskopf, *A three parameter study of external cavity modes in semiconductor lasers with optical feedback*, 5th IFAC Workshop on Time-Delay Systems, 2004.
[29] J. Sacher, D. Baums, P. Panknin, W. Elsässer, and E. O. Göbel, *Intensity instabilities of semiconductor lasers under current modulation, external light injection, and delayed feedback*, Phys. Rev. A, 45 (1992), pp. 1893–1905.
[30] H. Schuster and P. Wagner, *Mutual entrainment of two limit cycle oscillators with time delayed coupling*, Progr. Theor. Phys., 81 (1989), pp. 939–945.
[31] G. Stepán, *Retarded Dynamical Systems: Stability and Characteristic Functions*, Longman Scientific and Technical, London, UK, 1989.
[32] S. H. Strogatz, *Nonlinear Dynamics and Chaos*, Perseus Books, Reading, Massachusetts, 1994.
[33] S. H. Strogatz and I. Stewart, *Coupled oscillators and biological synchronization*, Sci. Am.,

269 (1993), pp. 68–75.

[34] A. A. Tager and K. Petermann, *High-frequency oscillations and self-mode locking in short external-cavity laser diodes*, IEEE J. Quantum Electron., 30 (1994), pp. 1553–1561.

[35] R. Vicente, J. Mulet, M. Sciamanna, and C. Mirasso, *Simple interpretation of the dynamics of mutually coupled semiconductor lasers*, Proc. SPIE, 5349 (2004), pp. 307–318.

[36] E. A. Viktorov, A. M. Yacomotti, and P. Mandel, *Semiconductor lasers coupled face-to-face*, J. Opt. B: Quantum Semiclass., 6 (2004), pp. L9–L12.

[37] E. Wille, M. Peil, I. Fischer, and Elsässer, *Dynamical scenarios of mutually delay-coupled semiconductor lasers in the short coupling regime in: 'semiconductor lasers and laser dynamics*, Proceedings of SPIE, 5452 (2004).

[38] M. Wolfrum and D. Turaev, *Instabilities of lasers with moderately delayed optical feedbackk*, Opt. Commun., 212 (2002), pp. 127–138.

[39] H.-J. Wünsche, S. Bauer, J. Kreissl, O. Ushakov, N. Korneyev, F. Henneberger, E. Wille, H. Erzgräber, M. Peil, W. Elsässer, and I. Fischer, *Dynamics of delay-coupled semiconductor lasers: the short coupling regime*, submitted, (2004).

[40] S. Yanchuk, K. Schneider, and L. Recke, *Dynamics of two mutually coupled semiconductor lasers: instantaneous coupling limit*, Phys. Rev. E, 69 (2004), p. 056221.